From Drought to Aridification: Land-cover fingerprints of a drying Chile

(This paper is a non-peer reviewed preprint submitted to EarthArXiv)

Francisco Zambrano[a], Anton Vrieling[b], Francisco Meza[c,d,e], Iongel Duran-Llacer[f], Francisco Fernández[g,h], Alejandro Venegas-González[i], Nicolas Raab[c], and Dylan Craven[j,k]

[a] DataGeo Insights, Santiago, Chile.

[b] Faculty of Geo-Information Science and Earth Observation (ITC), University of Twente, Enschede, The Netherlands.

[c] Facultad de Agronomía y Sistemas Naturales, Pontificia Universidad Católica de Chile., Santiago, Chile.

[d] Instituto para el Desarrollo Sustentable. Pontificia Universidad Católica de Chile, Santiago, Chile.

[e] Centro Interdisciplinario de Cambio Global, Pontificia Universidad Católica de Chile, Santiago, Chile.

[f] Escuela de Ingeniería en Medio Ambiente y Sustentabilidad y Escuela de Ingeniería Forestal, Facultad de Ciencias, Ingeniería y Tecnología, Universidad Mayor, Camino La Pirámide 5750, Santiago 8580745, Chile.

[g] Center of Economics for Sustainable Development (CEDES), Faculty of Economics and Government, Universidad San Sebastián, Santiago, Chile.

[h] Center of Applied Ecology and Sustainability (CAPES), Santiago, Chile.

[i] Instituto de Ciencias Agroalimentarias, Animales y Ambientales (ICA3), Universidad de O'Higgins, San Fernando, Chile.

[j] GEMA Center for Genomics, Ecology & Environment, Universidad Mayor, Camino La Pirámide Huechuraba 5750, Santiago, Chile.

[k] Data Observatory Foundation, Santiago, Chile.

Corresponding author. Email: francisco@datageoi.cl

Key Points

- Water-balance trends and vegetation shifts suggest Chile has crossed from episodic drought into persistent aridification
- This aridification, apparent from reduced soil moisture and evapotranspiration, is associated with vegetation loss and land cover shifts.
- Climate-driven aridification impacts vegetation, ecosystems, and land use—despite other factors like fires.

Abstract

Chile has endured a decade-long “mega-drought”, yet it remains unclear whether this represents a temporary climate anomaly or the onset of long-term aridification. While droughts are typically temporary events, persistent or recurrent droughts can indicate a transition toward aridification, i.e., a gradual shift to drier conditions. We assessed how temporal changes in water supply and demand at multiple time scales affect vegetation productivity and land cover changes in continental Chile to diagnose the region’s climate trajectory from drought to aridification. Since 2000, much of the region has seen a continuous decrease in water supply alongside a rise in atmospheric water demand. Further, in water-limited ecoregions, evapotranspiration, likely reflecting reduced transpiration or vegetation cover, has declined over time, with this trend intensifying over longer time scales. A long-term decline in water availability and shifting demand have led to declining vegetation productivity, especially in the Chilean Matorral and the Patagonia Steppe ecoregions. We discovered a link between these declines and drought indices related to soil moisture and actual evapotranspiration at time scales of up to 12 months. Further, our results indicate that the trends in drought indices account for up to 78% of shrubland and 40% of forest area changes across all ecoregions. The most important variable explaining cropland changes is the burned area. Our findings suggest that Chile is undergoing a transition from episodic drought to aridification, underscoring the need for adaptation strategies aligned with this emerging baseline.

Plain Language Summary

Climate change is not only increasing the frequency and severity of droughts—it is also leading to aridification by pushing certain regions toward a drier state and changing their ecosystem. In this study, we examined how changing patterns of water supply and demand are affecting vegetation and land cover across **continental Chile**, a region with diverse climates and ecosystems.

Using earth observation data and advanced drought indicators, we found that many areas—particularly the **Chilean Matorral and Patagonian steppe**—are experiencing

persistent drying. These changes are causing a **decline in vegetation productivity** and a shift in land cover, especially toward **drought-tolerant shrublands**. While human activities like wildfires also play a role, our results indicate that **aridification is strongly associated with** these transformations.

These findings highlight the need for **adaptive land management** and **ecosystem conservation strategies** that consider the long-term effects of a changing water balance—not just short-term drought events.

1. Introduction

Aridification is a gradual shift to drier conditions that affects global ecosystems and agri-food systems by causing land degradation, desertification, decreased crop yields, loss of biodiversity, and increased tree mortality (Pricope et al., 2025; Cheng et al., 2024; Vicente-Serrano et al., 2024). Further, across many regions of the world, droughts are becoming longer, more frequent, and more severe (Calvin et al., 2023; Gebrechorkos et al., 2025; Miranda et al., 2023). Yet, sometimes drought is confused with aridification, but they differ in that drought is a temporal anomaly, while the latter are long-term, persistent conditions characterized by consistently low water availability (Vicente-Serrano et al., 2025). Differentiating between drought and aridification is crucial for effective policy-making, resource management, and societal adaptation. Treating aridification as merely a prolonged drought can lead to inadequate and short-sighted solutions, ultimately exacerbating economic hardship and ecological degradation (Moss et al., 2024).

According to the (Shukla et al., 2019), aridification is a major climatic driver that exacerbates land degradation, especially in already water-limited regions. Addressing land degradation is crucial to secure food and water, mitigate climate change, and prevent conflict and migration, as its combined impacts with climate change could severely reduce crop yields, destabilize societies, and displace up to 700 million people by 2050 (Scholes et al., 2018). Nevertheless, identifying the threshold where aridification starts is complex due to its multidimensionality. These thresholds are commonly referred to as a "tipping point". In short, these points signify the transition between various system states, occurring when external conditions reach specific thresholds that trigger a rapid shift to a distinctly new

state (Dakos et al., 2019). (Berdugo et al., 2020) identifies three phases for ecosystem threshold: 1) reduction in vegetation productivity, 2) soil disruption, and 3) systematic breakdown. Most plant species can no longer withstand shortages in water and nutrient availability once they reach the third phase. Thus, aridification, driven by long-term declines in precipitation and increases in temperature, is a key climatic driver of land cover change, as it reduces vegetation productivity and accelerates the conversion of ecosystems into barren or sparsely vegetated areas (Shukla et al., 2019).

Expanding analyses to incorporate various climate dimensions can offer complementary insights into Earth's water balance and its impacts across multiple timescales. This approach could also aid in differentiating between drought and aridification. The World Meteorological Organization recommends the use of a single drought index for monitoring droughts (WMO et al., 2012), i.e., the multi-scale Standardized Precipitation Index (SPI; (Mckee et al., 1993), which is limited in that it only considers water supply in the form of precipitation. The Standardized Precipitation Evapotranspiration Index (SPEI; (Vicente-Serrano et al., 2010) builds upon the Standardized Precipitation Index (SPI) by incorporating the impact of temperature on drought through the use of atmospheric evaporative demand (AED), which is also referred to as potential evapotranspiration. It is now widely utilized for drought monitoring (e.g., (Gebrechorkos et al., 2023; X. Liu et al., 2024). Indices derived from soil moisture products (Narasimhan & Srinivasan, 2005; Souza et al., 2021), such as the Standardized Soil Moisture Index (SSI; (AghaKouchak, 2014; AghaKouchak et al., 2015) also monitor water supply and are thought to better capture water availability for crops, thus providing more relevant information for evaluating agricultural droughts. To disentangle the effects of precipitation from those of temperature (Vicente-Serrano et al., 2019), as well as to capture droughts in terms of water atmospheric demand, AED has been integrated into the Evaporative Demand Drought Index (EDDI; (Hobbins et al., 2016; McEvoy et al., 2016), which is particularly effective at detecting the rapid onset or intensification of droughts. To quantify the water loss by vegetation, one can use the actual evapotranspiration (ET), which is the amount of water removed by evaporation and transpiration. The Standardized Evapotranspiration Index (SETI; Yang et al., 2019) utilizes the anomaly of ET as a drought index to assess vegetation water loss. In

turn, ecological droughts, which capture the joint effects of precipitation and temperature in modifying natural and productive ecosystems (Camps-Valls et al., 2021; Helman et al., 2014; Paruelo et al., 2016), are complex to measure and can therefore be monitored using multiple drought indices, e.g., precipitation, temperature, evapotranspiration, and AED. Although such an approach accounts for the joint effects of changes in natural and productive ecosystems, its potential impacts on land cover change have been largely unexplored (Marumbwa et al., 2020; Tollerud et al., 2018).

From 1960 to 2019, land-use change has impacted approximately one-third of the Earth's surface, which is four times more than previously thought (Winkler et al., 2021). Water availability is responsible for approximately 55% of variability in vegetation productivity globally (Peng et al., 2017). However, the evidence supporting these results is derived from only one drought index, SPEI, which combines a proxy for water supply - precipitation - with a proxy for water demand - AED - at one time scale (12 months). The use of only one time scale may bias results of water availability impacts towards ecosystems dominated by plant growth forms such as grasses and herbs that respond more rapidly to drought stress (< 12 months). This is because physiological differences among and within dominant plant growth forms may increase (or decrease) tolerance of drought stress (Craine et al., 2013; McDowell et al., 2022). For example, trees growing in more arid ecosystems typically respond over longer time scales than those in more humid ecosystems (Vicente-Serrano et al., 2014). Another source of uncertainty regarding water availability impacts on land cover change and vegetation productivity are extrinsic factors, such as large-scale public policy (e.g., national and international reforestation initiatives), agricultural practices (e.g., clearing forest for soybean or oil palm), and rural and urban land use planning (Karabulut et al., 2023).

Climate projections suggest that some parts of the world including Chile may experience significant aridification (Mirzabaev et al., 2022). Here, to differentiate between drought and aridification, we will use the definition provided by Lisonbee et al. (2025). According to this definition, when the impacts of a prolonged drying period surpass the resilience of a system and lead to permanent changes, e.g., ecological transformation, the drying process is categorized as aridification. Thus, to enhance our understanding of the multidimensional

impacts of climate change on the temporal dynamics of natural and productive ecosystems, we evaluate temporal changes in water supply and demand, net primary productivity, and land-cover change across terrestrial ecosystems for 2000-2023. Chile's diverse climate and ecosystems (Beck et al., 2023; Luebert & Pliscoff, 2022) make it an ideal natural laboratory for assessing the dynamic interactions between climate and ecosystems, and potential impacts on land-cover change. Additionally, large parts of Chile have experienced severe drought conditions that have significantly affected vegetation and water storage in recent years; central Chile has faced a persistent precipitation deficit (or "mega-drought") since 2010 (R. Garreaud et al., 2017), which strongly impacted native forests (e.g., (Miranda et al., 2020; Urrutia-Jalabert et al., 2018; Venegas-González et al., 2018) and agricultural productivity (e.g., (Zambrano et al., 2016, 2018; Zambrano, 2023b). However, this prolonged extreme drought may be hiding an aridification that could be responsible for changes in land cover, altering the provision of key ecosystem services and agricultural production. Here, we explicitly test the hypothesis that the recent "mega-drought" in Chile is the climate expression of an ongoing aridification process. We will test the hypothesis by assessing short- to long-term time trends (1 to 36 months) in water availability using multi-scalar drought indices that capture variation in the components of water balance, i.e., water supply (SPI, SPEI, SSI) and demand (EDDI, SETI), and their impacts on vegetation productivity and land cover change across continental Chile.

We believe that drought indices can help us find the drying trend, i.e., aridification, that is causing a decrease in vegetation productivity and the change in land cover, and that these effects will be more severe for soil moisture (L. Liu et al., 2020) (i.e., SSI) and evapotranspiration (Hong et al., 2023) (i.e., SETI). We further assess the relative influence of water availability at multiple temporal scales on land cover change, relative to human activities that may indirectly influence water demand, across ecoregions experiencing shifts in water demand and supply of varying intensity and duration. Our integrative approach assesses climate change impacts by combining multiple dimensions of the water balance—such as water supply and demand—across multiple time scales and evaluating their effects on vegetation productivity and land cover change. This framework intends to deepen our understanding of climate-driven ecosystem changes worldwide.

2. Materials and Methods

2.1. Study area

Continental Chile has a diverse climate, with strong environmental gradients from north to south and east to west (Aceituno et al., 2021) (Fig. 1a), which, together with its complex topography (Fig. 1b), determine its ecosystem diversity (R. D. Garreaud, 2009; Luebert & Pliscoff, 2022) (Fig. 1c). We therefore divided Chile into ecoregions (Dinerstein et al., 2017), which are regions that share similar geography and ecology, and have comparable levels of precipitation and solar radiation. Seven ecoregions were identified: Atacama desert, Central Andean dry puna, Southern Andean steppe, Chilean Matorral, Valdivian temperate forests, Magellanic subpolar forests, and Patagonian steppe. The Atacama desert is predominantly arid with hot (Bwh in the Koppen-Geiger classification) and cold (Bwk) temperatures, as well as the northern part of the Chilean Matorral. Most of the land in these two northern regions is bare, except for a small area where shrublands and grasslands are present. With an annual rainfall of less than 400 mm, the Central Andean dry puna ecoregion has low, yet highly seasonal precipitation with an eight-month dry season, low temperatures (Bwk) and is dominated by grasslands, shrublands, and savanna. The climate of the Southern Andean steppe ecoregion is cold desert (BWk), with most precipitation occurring in the winter. There is little vegetation in this ecoregion because the plants have adapted to its windy, dry, and cold climate. In central Chile, the climate of the Chilean Matorral changes to that of an arid steppe with cold temperatures (Bsk). Then, towards the center-south of the country, the climate of the Chilean Matorral changes to a Mediterranean climate, with warm to hot summers (Csa and Csb). Land cover in this ecoregion consists of a significant amount of shrublands and savannas. The Valdivian temperate forests have a mostly oceanic climate (Cfb) and a large area of forests and grasslands. The Magellanic subpolar forests have a tundra climate. Lastly, the Patagonian steppe has high aridity, cold temperatures (Bsk), and primarily consists of grasslands.

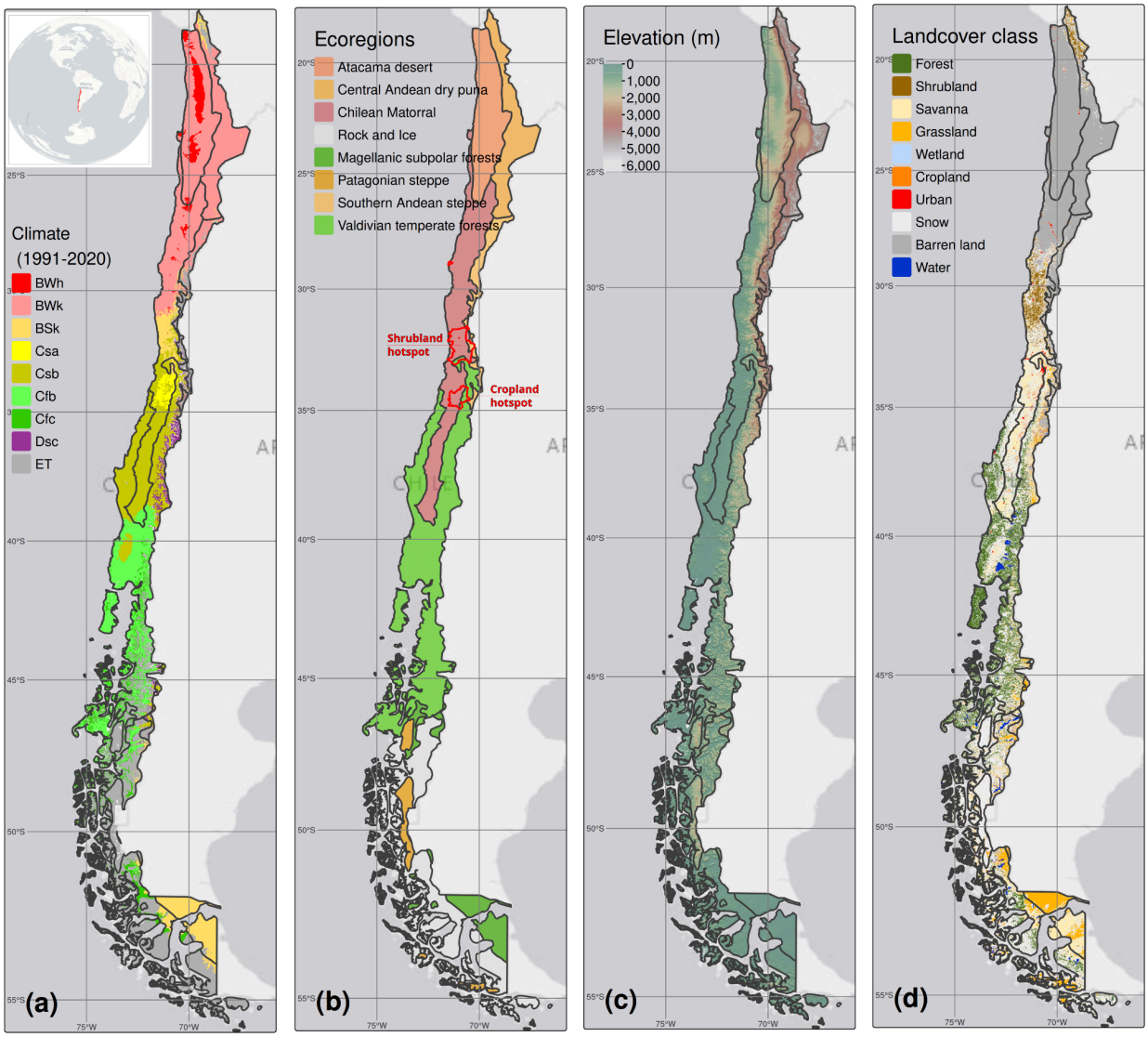

Figure 1. Climate, topography, and land cover classes across continental Chile. Koppen-Geiger climate classes (**a**), ecoregion's map highlighting the hotspots for trends in cropland and shrubland (outlined in red), (**b**), topography (**c**), and persistent land cover classes (> 80%) for 2001-2023 (**d**) across continental Chile.

2.2. Data

2.2.1. Gridded meteorological and vegetation data

To derive a proxy for vegetation productivity, we used the Normalized Difference Vegetation Index (NDVI) from the MOD13A3 (Didan, 2015) Collection 6.1 product derived from the MODIS (Moderate-Resolution Imaging Spectroradiometer) sensor onboard the Terra satellite. MOD13A3 provides vegetation indices with a 1 km spatial resolution and monthly

frequency (Didan, 2021). We also utilized monthly actual evapotranspiration (ET) retrievals at a ~500m spatial resolution from the MOD16A2 Collection 6.1 (Running et al., 2017) product to assess the water consumption of vegetation. For soil water availability, water supply, and water demand variables, i.e., soil moisture, precipitation, AED, and evapotranspiration, we used ERA5-Land (ERA5L; ECMWF Reanalysis version 5 over land)(Muñoz-Sabater et al., 2021), a reanalysis dataset that provides atmospheric and land variables since 1950. It has a spatial resolution of 0.1° (9 km), hourly frequency, and global coverage. We selected total precipitation, maximum and minimum temperature at 2 meters, and volumetric soil water layers between 0 and 100 cm of depth (see Table S1 & S3).

2.2.2. Gridded indicators for human impacts on land use

To analyze land cover change, we used the classification scheme of the International Geosphere-Biosphere Programme (IGBP) from the product MCD12Q1 Collection 6.1 (Friedl & Sulla-Menashe, 2019) from MODIS. This product is produced for each year from 2001 to 2023 and defines 17 classes (see Table S1). To account for the impacts of human activity on land cover change, we obtained data on road density (Meijer et al., 2018), total burned area, and nighttime light emissions for the period 2012–2023 (Román et al., 2018). These products are frequently used to quantify the human footprint (e.g., (Halpern et al., 2008, 2015) or biodiversity threats (e.g., (Bowler et al., 2020; Kennedy et al., 2019). To capture changes in land cover due to fires, we calculated the total burned area and the trend for 2002-2023 (Chen et al., 2023). For nighttime light emissions, we calculated the trend and the average annual nighttime light emissions.

2.3. Short- to long-term drought trends

2.3.1. Atmospheric Evaporative Demand (AED)

To quantify water demand using drought indices, we first calculated atmospheric evaporative demand (AED). To calculate AED, the most reliable method is the FAO Penman-Monteith (Allen et al., 2011), but it has the drawback that it depends on several variables. As a surrogate of the Penman-Monteith, the Hargreaves-Samani method was proposed (G. H. Hargreaves, 1994; G. L. Hargreaves & Samani, 1985) due to its accuracy, consistency, and parsimonious nature. We selected the Hargreaves method for estimating

AED because of its simplicity, as it only requires temperature and extraterrestrial radiation. We used it as follows:

$$AED = 0.0023 \cdot Ra \cdot (T + 17.8) \cdot \left(T_{max} - T_{min}\right)^{0.5}, (Eq.\ 1)$$

where Ra $\left(MJm^{2}day^{-1}\right)$ is extraterrestrial radiation and T, T_{max}, and T_{min} are mean, maximum, and minimum temperature ($°C$) at 2 m, respectively. For calculating Ra we used the coordinate of the latitude of the centroid of each pixel as follows:

$$R_a = \frac{14{,}400}{\pi} \cdot G_{sc} \cdot d_r[\omega_s \cdot sin(\phi) \cdot sin(\delta) + cos(\phi) \cdot cos(\delta) \cdot sin(\omega_s)] \text{ (Eq. 2)},$$

where:

Ra: extraterrestrial radiation ($MJm^{-2}day\ -\ 1$),

G_{sc}: solar constant = 0.0820 ($MJm^{-2}min^{-1}$),

d_r: inverse relative distance Earth-Sun,

ω_s sunset hour angle (rad),

ϕ: latitude (rad), and

δ: solar declination (rad).

2.3.2. Drought indices

To derive the drought indices of water supply and demand, we used the ERA5L with a monthly frequency for 2000–2023. Drought indices capture historical anomalies of water supply and demand. To quantify each anomaly, the common practice is to derive it following a statistical parametric method in which it is assumed that the statistical distribution of the data is known (Heim, 2002). The use of an erroneous statistical distribution that does not fit the data is usually the highest source of uncertainty (Laimighofer & Laaha, 2022). In the case of Chile, due to its high degree of climatic variability, it is difficult to choose a statistical distribution that can be used across its entire extent. We therefore used a non-parametric method for the calculation of the drought indices, following (Farahmand & AghaKouchak, 2015).

For monitoring water supply, we used the Standardized Precipitation Index (SPI; (McKee et al., 1995), which only uses precipitation data. To evaluate water demand, we chose the Evaporative Demand Drought Index (EDDI; (Hobbins et al., 2016; McEvoy et al., 2016), which is based on AED, and the Standardized Evapotranspiration Index (SETI; (Paruelo et al., 2016), which quantifies actual evapotranspiration, i.e. the amount of water removed from a surface due to evaporation and transpiration. To quantify the combined effect of water supply and demand, we estimated SPEI (Vicente-Serrano et al., 2010). For SPEI, we calculated an auxiliary variable (D) according to:

$$D = P - AED \; (Eq.\ 3),$$

where P is precipitation. Soil moisture is often considered to be the main driver of vegetation productivity, particularly in semi-arid regions (Li et al., 2022). Hence, we used the Standardized Soil Moisture Index (SSI) to analyze the change in soil moisture (SM)(Hao & AghaKouchak, 2013). For SSI, we used the average soil moisture from ERA5L in the first meter below the soil. All calculated indices are multi-scalar and can be used for the analysis of short- to long-term droughts.

To derive the drought indices, we first calculated the sum of the variables for each time scale(s). In this case, for generalization purposes, we use V, referring to variables P, AED, D, ET, and SM (see Table S2). We summed each variable over the time series (months), for a time scale s:

$$A_i^s = \sum_{i=n-s-i+2}^{n-i+1} V_i \forall i \geq n - s + 1 \; (Eq.\ 4)$$

A_i^s corresponds to a moving window (convolution) that sums the variable over s months, starting from the most recent month (n) back in time until month n-s+1. For example, using precipitation, a period of twelve months (n), and a time scale of three months (s):

$$A_1^3 = P_{oct} + P_{nov} + P_{dic}$$

$$\vdots \quad = \quad \vdots \quad + \quad \vdots \quad + \quad \vdots$$

$$A_{10}^{3} = P_{jan} + P_{feb} + P_{mar}$$

Then, we used the empirical Tukey plotting position (Wilks, 2011) over A_i^s to derive the $P\left(a_i\right)$ probabilities across a period of interest:

$$P\left(A_i^s\right) = \frac{i-0.33}{n+0.33'} \ (Eq.\ 5)$$

We use an inverse normal approximation (Abramowitz & Stegun, 1968) to obtain the empirically derived probabilities once the variable accumulates over time for the scale *s*. Thus, the drought indices SPI, $SPEI$, $EDDI$, $and\ SSI$ are obtained in the following manner:

$$DI\left(A_i^s\right) = W - \frac{C_0+C_1 \cdot W+c_2 \cdot W^2}{1+d_1 \cdot W+d_2 \cdot W^2+d_3 \cdot W^3}, \ (Eq.\ 6)$$

where DI refers to the drought index calculated for the variable V. The values for the constants, based on (Abramowitz & Stegun, 1968), are: $C_0 = 2.515517$, $C_1 = 0.802853$, $C_2 = 0.010328$, $d_1 = 1.432788$, $d_2 = 0.189269$, and $d3 = 0.001308$. For $P\left(A_i^s\right) \leq 0.5$, W=$\sqrt{-2 \cdot ln\left(P\left(A_i^s\right)\right)}$, and for $P\left(A_i^s\right) > 0.5$, replace $P\left(A_i^s\right)$ with $1 - P\left(A_i^s\right)$ and reverse the sign of $DI\left(A_i^s\right)$.

The drought indices were calculated for time scales of 1, 3, 6, 12, 24, and 36 months at a monthly frequency for 2000–2023.

2.4. Temporal trends of drought indices

To determine if there are statistically significant positive or negative temporal trends for the drought indices, we used the non-parametric modified Mann-Kendall test for serially correlated data (Yue & Wang, 2004). To determine the magnitude of the trend, we used Sen's slope (Sen, 1968). Sen's slope is less affected by outliers than parametric ordinary least squares (OLS) regression, and as a non-parametric method, it is not influenced by the distribution of the data. We applied both methods for SPI, EDDI, SPEI, SETI, and SSI and six

time scales, resulting in a total of 30 trends. We then aggregated temporal trends for each ecoregion and land cover type.

The trends in the drought indices will help us to evaluate if there is aridification. As droughts are temporal anomalies, they should not have a trend, and their value should be around zero. However, if a trend exists and intensifies over longer time scales—such as an increase in AED and a decrease in water supply—it will clearly indicate drying conditions related to aridification.

2.5. Vegetation productivity

We also used the MODIS product (MOD13A3; (Didan, 2021), as a proxy of vegetation productivity. We calculated anomalies of cumulative NDVI using zcNDVI (Zambrano et al., 2018), which was derived from the monthly time series of NDVI, with Equations 3, 4, 5 and 6. For vegetation productivity, we selected the time scale that best correlates with annual net primary productivity (NPP) across continental Chile. For this purpose, we calculated zcNDVI for time scales of 1, 3, 6, and 12 months (in December) and compared it with the annual NPP. We obtained NPP from MOD17A3HGF (Running & Zhao, 2019). Based on this comparison, we selected six months because it resulted in the highest R^2 between zcNDVI and NPP, i.e. 0.31 for forest and 0.72 for shrubland (see Figs. S1 & S2). We subsequently used zcNDVI with a time scale of 6 months and calculated it at a monthly frequency for 2000–2023.

2.6. Climate impacts on vegetation productivity

For each land cover type, we analyzed the trend of vegetation productivity. To this end, we identified areas with a persistent land cover over time (80% of the years) to reduce the possibility that trends in vegetation productivity may be influenced by changes in land cover. We examined the correlation between drought indices and vegetation productivity across land cover types to determine the extent to which soil moisture and water demand and supply affect vegetation productivity.

We estimated pixel-to-pixel Pearson's correlations between drought indices at time scales of 1, 3, 6, 12, 24, and 36 months with zcNDVI. We extracted the Pearson correlation coefficient corresponding to the time scale with the highest value. For each index, we then generated two maps: 1) a raster with values of the time scales and drought index that reached the maximum correlation (see Fig. S5), and 2) a raster with the magnitude of the correlation between the drought index and vegetation productivity.

2.7. Climate impacts on land cover change

2.7.1. Land cover change

Following the FAO classification (FAO, 2022), we classified native and planted forests as "forests", which represent natural and productive ecosystems dominated by large trees. To analyze the land cover change, we use the IGBP scheme from the MCD12Q1 product. We regrouped the 17 classes into ten macro-classes, as follows: 1-4 to forests (native forest and plantations), 5-7 to shrublands, 8-9 to savannas, 10 as grasslands, 11 as wetlands, 12 and 14 to croplands, 13 as urban, 15 as snow and ice, 16 as barren, and 17 as water (see Table S1). This resulted in a time series of land cover with ten macro-classes for 2001-2023. We validated the land cover macro-classes using a high resolution (30 m) land cover map for 2013-2014 (Zhao et al., 2016). Our results showed a global accuracy of ~0.82 and a F1 score of ~0.66 (Supplementary Information, section S2).

We did not directly measure the change in land cover, but we analyzed it indirectly. A decrease in one type of land cover leads to its replacement by another, and an increase in a particular land cover class means it is replacing other types of covers. Thus, we calculated the area for each land cover class in each ecoregion for 2001–2023. We then estimated the temporal change in area for each land cover type and determined the statistical significance (p-value < 0.05) and magnitude of the trend, as described above.

To assess how water demand and supply and soil moisture affect variation in vegetation productivity across various land cover types, we avoided analyzing areas that experienced major land cover changes during the study period. To assess how zcNDVI varied irrespective of land cover change, we developed a persistence mask for land cover, which

only retains pixels for those whose land cover remained the same for at least 80% of the 23 years (Fig. 1d).

2.7.2. Relationship between land cover and drought indices trends

We evaluated changes in land cover across continental Chile with the Random Forest algorithm and using drought indices at multiple time scales and temporal trends in road density, burned area, and nighttime light emissions. We performed the analysis at the sub-basin scale, using a total of 485 river basins, which have a surface area between 0.906 and 24,408 km^2 and a median area of 1,249 km^2 (see Fig. S3/Table S4). For each basin, we calculated the temporal trend per land cover, considering the proportion of the type relative to the total surface of the basin. For each basin we extracted the average trend of all drought indices and at time scales of 1, 3, 6, 12, 24, and 36 months. In the case of burned area, we used as variables the total and the trend of burned area for 2002-2023, and for nighttime light emissions we used the average and the trend for 2012-2023.

Prior to fitting models, we assessed multi-collinearity among explanatory variables, i.e., drought indices, road density, nighttime light emissions, and burned area, with the variance inflation factor (VIF). Because VIF values greater than five may affect the interpretation of model results (Dormann et al., 2013), we excluded SPI from all subsequent models (see Fig. S6-S11).

We used Random Forest models (Ho, 1995), as they capture non-linear relationships and minimize overfitting. For each combination of time scale (1, 3, 6, 12, 24, and 36 months) and land cover type (forest, grassland, shrubland, savanna, cropland, and barren land), we fitted a model with the following explanatory variables: trends of each drought index (SPI, SPEI, EDDI, SETI, and SSI), nighttime light emission (trends and averages), burned area (trends and total area), and road density. We trained each model using 1,000 trees, setting the minimum number of nodes per decision tree at five and the number of predictors per split (boosting) to the square root of the total number of predictors. To account for uncertainty, we trained all the models ten times using a resampling strategy (ten folds) in a cross-validation scheme. Finally, we evaluated model fit by calculating R^2, root mean square

error (RMSE), and variable importance. Variable importance identifies which variables have a higher contribution to explaining model variation. We calculated variable importance by permuting out-of-bag (OOB) data per tree and calculating the mean standard error of the OOB data. After permuting each predictor variable, we repeated the process for the remaining variables. We repeated this process ten times per model (ten folds) to assess model fit while accounting for uncertainty in model performance.

2.8. Software

For downloading, processing, and analyzing spatio-temporal data, we used the R programming language for statistical computing and graphics (R Core Team, 2025). For downloading ERA5L, we used the {ecmwfr} package (Hufkens et al., 2019). For processing raster data, we used {terra} (Hijmans, 2023) and {stars} (Pebesma & Bivand, 2023). For managing vectorial data, we used {sf} (Pebesma, 2018; Pebesma & Bivand, 2023). For the calculation of AED, we used {SPEI}(Beguería et al., 2014; Beguería & Vicente-Serrano, 2023). For mapping, we used {tmap}(Tennekes, 2018). For data analysis and visualization, the suite {tidyverse}(Wickham et al., 2019) was used. For the random forest modeling, we used the {tidymodels}(Kuhn & Wickham, 2020) and {ranger}(Wright & Ziegler, 2017) packages.

3. Results

3.1. The Chilean matorral and Patagonian steppe increase atmospheric water demand but decrease evapotranspiration

We found that the majority of the drought indices indicate that the temporal trends (positive or negative) intensify over longer time scales (Fig. 2). For the Atacama Desert and the Central Andean dry puna, we found a positive temporal trend for drought indices of water supply (i.e., SPI and SSI), atmospheric water demand (i.e., EDDI), and evapotranspiration (i.e., SETI). For the Chilean Matorral and Patagonian steppe, EDDI becomes increasingly positive, while SPI, SPEI, SSI, and SETI become increasingly negative. This reflects a critical climatic scenario, where a rise in temperature increases atmospheric water demand, but actual evapotranspiration cannot increase due to a lack of water

availability. In the Southern Andean steppe, there is a positive temporal trend in AED (i.e., EDDI), but a negative temporal trend in water supply (i.e., SPI, SPEI, SSI). The negative temporal trend in vegetation water demand (i.e., SETI) strengthens with longer time scales. The Valdivian temperate forests show a negative temporal trend in water supply (i.e., SPI, SPEI, and SSI) and a positive trend in both AED and ET, as shown by EDDI and SETI, respectively. In this case, an increase in AED implies an increase in ET, likely due to a greater availability of water, unlike in the Chilean Matorral and Patagonian steppe. The vegetation water demand (SETI) in the Magellanic subpolar forests does not exhibit a significant trend over any given time scale, while AED and water supply become increasingly positive over longer time scales. The trends of drought indices in the Patagonian steppe exhibit a similar behavior to the Chilean Matorral, albeit less extreme.

The bottom panels in Fig. 2 illustrate the behavior of drought indices for the selected subbasins, which are in the 5% quantile for an increasing trend in shrubland (shrubland hotspot) and a 5% quantile for a decreasing trend in cropland surface (cropland hotspot). In these cases, the pattern observed in the "Chilean Matorral" is more pronounced. But, as could be expected, in the "cropland hotspot", the indices linked to soil moisture (SSI) and evapotranspiration (SETI) have lower values in comparison with the "shrubland hotspot". This decrease is likely to be due to the fact that cropland receives water through irrigation.

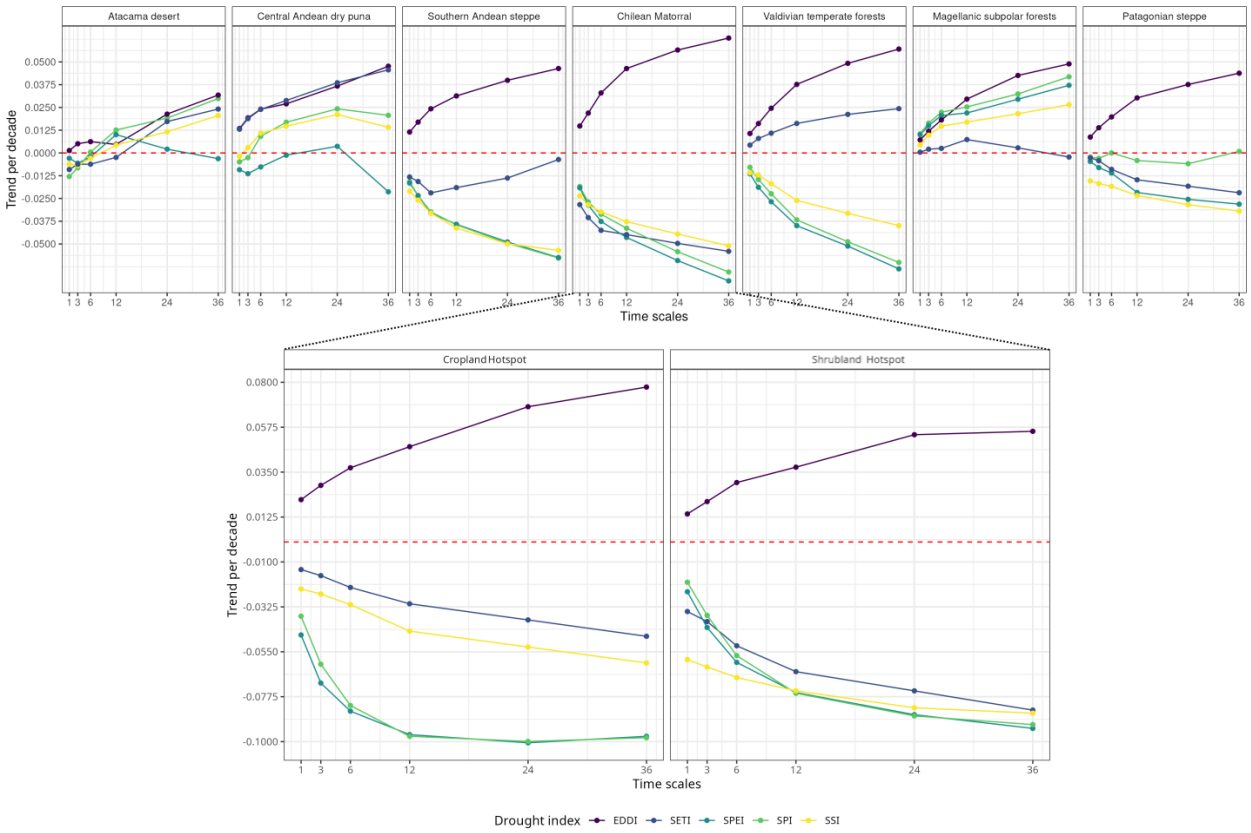

Figure 2. The Chilean Matorral and Patagonian steppe show a higher increase in atmospheric water demand and a decrease in vegetation evapotranspiration, which becomes stronger at longer time scales. Top row: temporal trends in drought intensity over multiple time scales for indices associated with water supply (SPI, SPEI, SSI), atmospheric water demand (EDDI) and vegetation water demand (SETI) across continental Chile for 2000-2023. Bottom row: highlights the trends in drought intensity for the "Cropland hotspot" and "Shrubland hotspot". SPI is the standardized precipitation index, SPEI is the Standardized Precipitation Evapotranspiration Index, SSI is the Standardized Soil Moisture Index, EDDI is the Evaporative Demand Drought Index, and SETI is the Standardized Evapotranspiration Index. Drought indices were aggregated per region for visualization. All temporal trends are statistically significant ($p < 0.05$).

3.2. The proxy of vegetation productivity has strongly decreased in the Chilean matorral and the Patagonian steppe

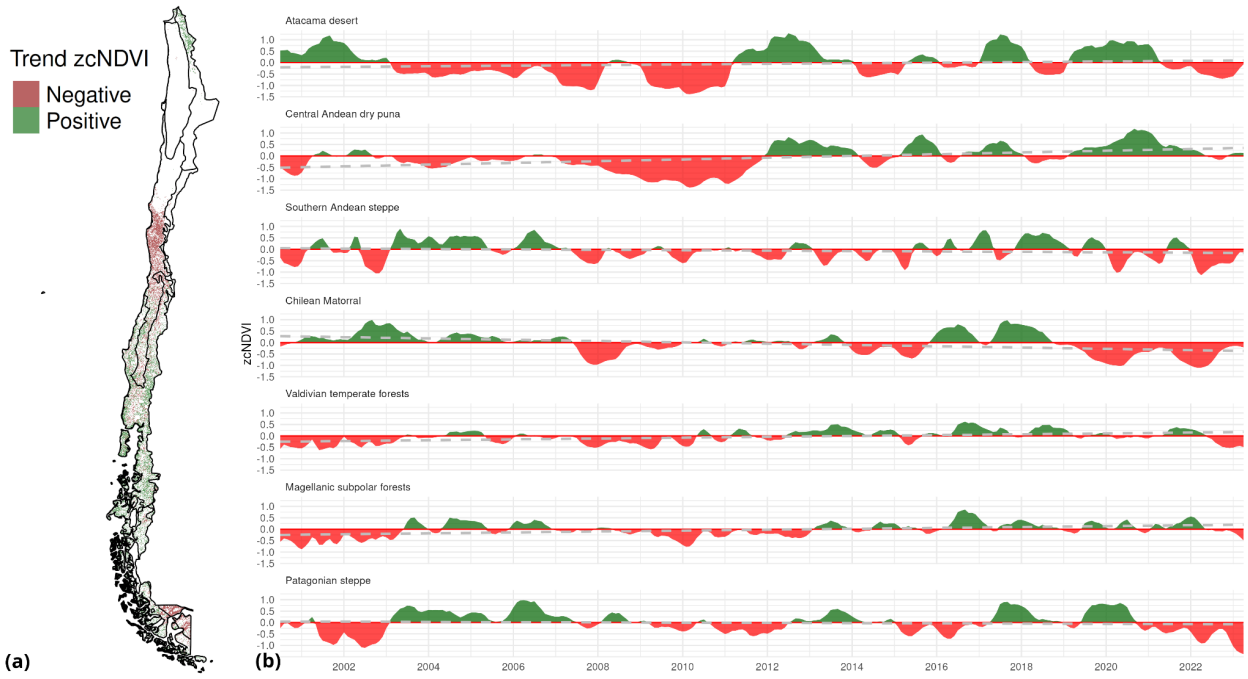

Figure 3. The Chilean matorral and Patagonian steppe have experienced the greatest decline in the proxy of vegetation productivity. Spatial (**a**) and temporal (**b**) variation in vegetation productivity (zcNDVI) across continental Chile for 2000-2023. In (**a**), green corresponds to areas with a positive temporal trend in zcNDVI, and red corresponds to a negative temporal trend in zcNDVI. White represents areas without persistent land cover, or areas where there is no statistically significant trend in zcNDVI. All temporal trends shown are statistically significant ($p < 0.01$). In (**b**), red areas correspond to negative and green to positive zcNDVI anomalies. Temporal trends in zcNDVI were estimated with the non-parametric modified Mann-Kendall test for serially correlated data.

We found contrasting temporal trends in the proxy of vegetation productivity for 2000-2023 across ecoregions (Figs. 3 & S4). While the Atacama desert does not exhibit significant temporal trends in zcNDVI, that of the Chilean Matorral, Patagonian steppe, and the Southern Andean steppe exhibit negative trends of -0.023, -0.016, and -0.006 (z-score per decade), respectively. In contrast, the Central Andean dry puna, Valdivian temperate forests, and Central Andean dry puna show positive temporal trends in zcNDVI ranging from 0.01 to 0.03 (z-score per decade). The Chilean Matorral reached its lowest point from

2019 to 2022, while the Patagonian steppe has experienced an increasingly negative trend in the proxy of vegetation productivity since 2022.

3.3. Forest, savanna, and shrubland exhibit the highest change in surface area across ecoregions

We observed significant changes in land cover across continental Chile (Fig. 4). The forest surface area increased in the Chilean matorral and in the Valdivian temperate forest at rates of 78 and 316 km^2 yr^{-1}, respectively. Grassland surface area has diminished in the Southern Andean steppe (-19 km^2 yr^{-1}), yet has increased in the Patagonian steppe (90 km^2 yr^{-1}). Savanna has decreased rapidly in the Chilean matorral at a rate of -271 km^2 yr^{-1} and in the Valdivian temperate forest at a rate of -276 km^2 yr^{-1}, but has increased at a rate of 133 km^2 yr^{-1} in the Magellanic subpolar forest. Among land cover types, shrubland surface area has increased the most in the Chilean matorral (160 km^2 yr^{-1}). Barren land has increased at moderate rates in the Central Andean dry puna (36 km^2 yr^{-1}) and the Southern Andean steppe (50 km^2 yr^{-1}), but has diminished in the Magellanic subpolar forest (-81 km^2 yr^{-1}).

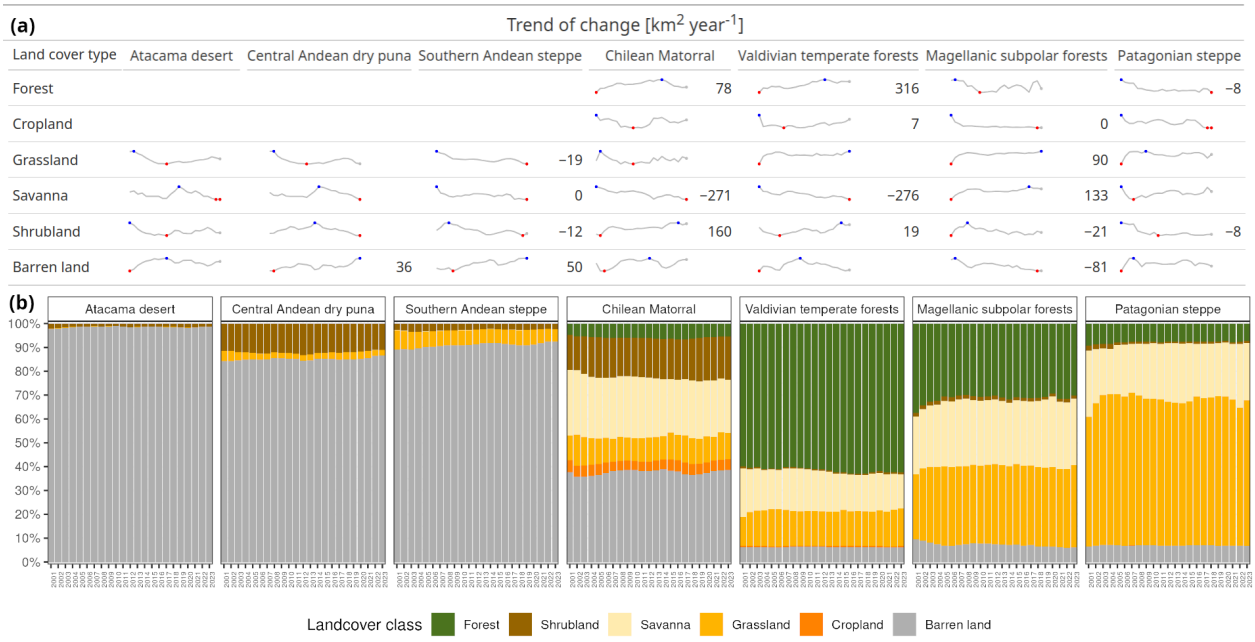

Figure 4. **Land cover is shifting dynamically across continental Chile**. Temporal trends in absolute (**a**) and relative (**b**) land cover change in surface area across continental Chile for 2001-2023. Temporal change in surface area for each land cover was estimated with Sen's slope; zero values indicate no change, curves

without values show no statistically significant trend, and red and blue points indicate maximum and minimum values, respectively. Land cover classes with no values indicate that it is not present in a given ecoregion. Relative land cover change was estimated within each ecoregion.

3.4. Drying trends' impacts on the proxy of vegetation productivity are strongest in the Chilean Matorral and Valdivian temperate forest

Our results indicate that the drying trends' impacts on vegetation productivity are highest in the Chilean Matorral and Valdivian temperate forests across all land cover types, except forest (Figs. 5 & S5 and Table 1). For time scales of 6 and 12 months, SETI and SSI have the strongest positive correlation with vegetation productivity among the land cover types. We found that vegetation productivity in grassland and savanna in the Patagonian steppe had higher correlations with SPI and SSI over a time scale of 12 months than other drought indices. Further, we found a positive, statistically significant relationship between vegetation productivity in the Atacama desert and drought indices of 12 months of water supply and demand (SPI, SPEI, SETI, and SSI) yet is a negative relationship between vegetation productivity and atmospheric water demand (EDDI) over a time scale of 12 months. All drought indices show a positive correlation with vegetation productivity in the Central Andean dry puna, particularly for the drought indices of water supply (SPI, SPEI, and SSI) at a time scale of 24 months and vegetation water demand (SETI) at a time scale of 36 months. For the Southern Andean steppe, SETI at a time scale of 24 months showed the highest correlation with vegetation productivity in savannas, followed by the EDDI at a time scale of 24 months.

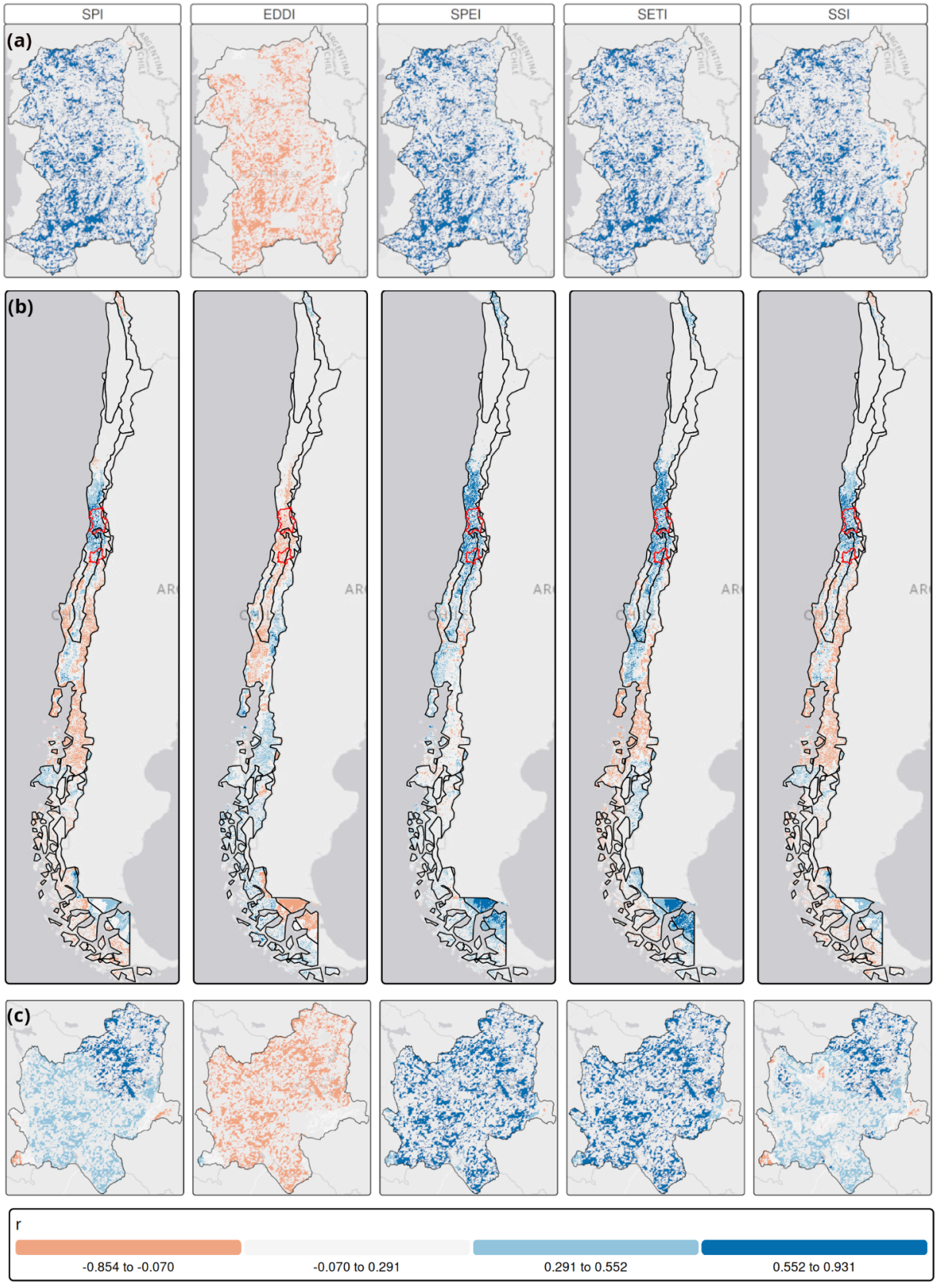
SPI
EDDI
SPEI
SETI
SSI
(a)
(b)
(c)
r
-0.854 to -0.070
-0.070 to 0.291
0.291 to 0.552
0.552 to 0.931

Figure 5. Aridification impacts on vegetation productivity shift across continental Chile. Pearson's correlation coefficient was used to estimate the direction and magnitude of the relationship between drought severity and vegetation productivity for each index for 2000-2023. We show Pearson correlation coefficients for the time scale (3 - 36 months) at which they reach their maximum absolute value. In Chile, areas in white indicate no statistically significant correlation (p-value>0.05). The panels show a) a zoom-in of the shrubland hotspot, b) continental Chile, and c) a zoom-in of the cropland hotspot. SPI is the standardized precipitation index, SPEI is the Standardized Precipitation Evapotranspiration Index , SSI is the Standardized Soil Moisture Index, EDDI is the Evaporative Demand Drought Index, and SETI is the Standardized Evapotranspiration Index.

Our analysis also revealed that water demand and supply differentially affected the time scales at which vegetation productivity of land cover types within each region was most impacted by drought (Figs. 5 & S5 and Table 1). While the spatial variation in the relationship between drought intensity and vegetation productivity was consistent across drought indices, the drought indices that captures water supply *via* soil moisture (Standardized Soil Moisture Index; SSI), and *via* evapotranspiration (Standardized Evapotranspiration Index, SETI) tended to show a stronger correlation with vegetation productivity over larger areas than the other drought indices (Fig. 5 & Table 1).

Table 1. Time scale at which drought indices (EDDI, SPI, SPEI, SSI, and SETI) exhibit the maximum absolute correlation with vegetation productivity (zcNDVI) across continental Chile. Values in each cell indicate the time scale in months (1, 3, 6, 12, 24, and 36 months) at which the maximum absolute correlation between a drought index and zcNDVI occurs, and the color indicates the strength of the correlation. Cells without values signify that either the correlation was not statistically significant, or that a given land cover type is not present in a particular ecoregion.

	Forest					Cropland					Grassland					Savanna					Shrubland				
Ecoregion	EDDI	SPEI	SPI	SSI	SETI	EDDI	SPEI	SPI	SSI	SETI	EDDI	SPEI	SPI	SSI	SETI	EDDI	SPEI	SPI	SSI	SETI	EDDI	SPEI	SPI	SSI	SETI
Atacama desert											12	12	12	12	12	6	12	12		12	12	12	12	12	12
Central Andean dry puna											12	36	36	36	36	24	36	36	36	36	12	36	36	36	12
Southern Andean steppe											24	12	12	6	6	24	12	12	6	24	6	36	36	36	6
Chilean Matorral	6	6	6	6	6	6	12	12	6	6	36	24	24	12	12	6	12	12	6	6	36	24	24	12	12
Valdivian temperate forests	6	6	6	12	36	6	6	6	6	6	6	12	12	12	6	6	6	24	6	6	36	12	12	12	12
Magellanic subpolar forests	6		36	6	6	12	12	12	36	24	6	12	12	6	6	6	6	6	6	6	6	6	6	36	6
Patagonian steppe	6	6	12	36	12						12	12	12	12	12	36	12	12	12	24		12	12	36	

Pearson correlation -0.75 -0.40 -0.05 0.30 0.65

3.5. Drying trends strongly impact land cover distribution for shrublands

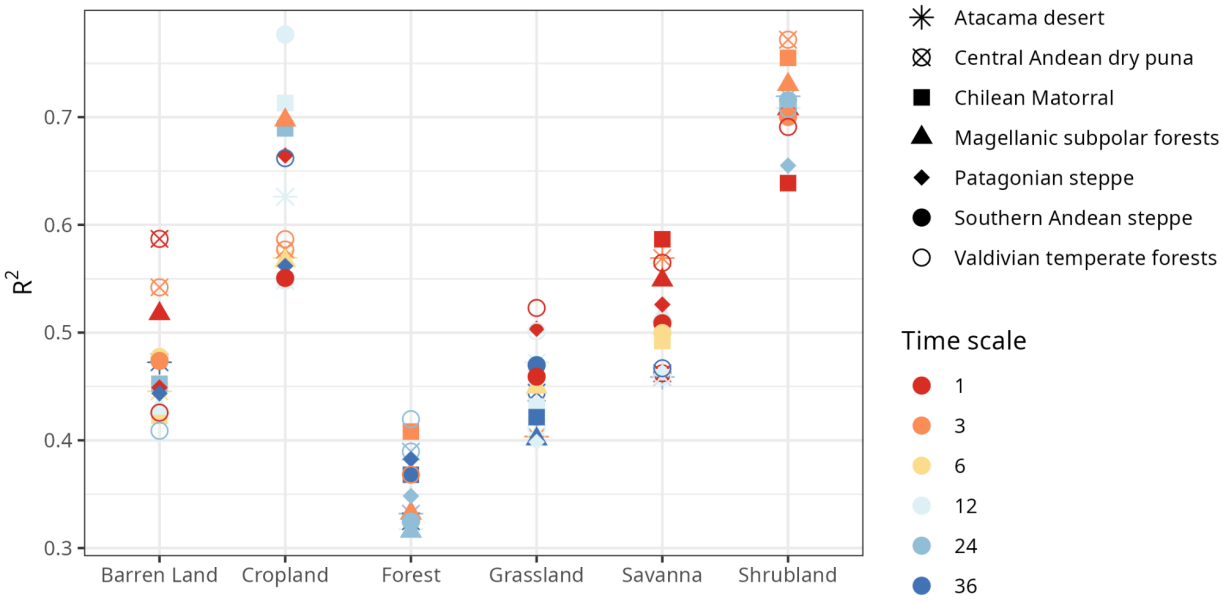

Figure 6. Shifts in shrubland areas are best explained by trends in drought indices at time scales of three and 12 months. R^2 values were estimated with random forest models for each land cover class and time scale.

Our random forest models explain between 32-79% of variation in the temporal trend of land cover change across continental Chile (Fig. 6). These results highlight the importance of considering water supply (e.g., SPEI and SSI) and demand (e.g., SETI), as climatic indices associated with both aspects of the water balance had high importance values across most ecoregions and land cover types. The variation in the time scale of drought indices with high importance values suggests that some types of vegetation rapidly respond to changes in water availability, while others are more resistant and likely adapted to more arid conditions (Fig. 6).

Our random forest models show that the drought indices explain between 71 and 78% of the variation in temporal trends of land cover surface change for shrublands across all ecoregions (Fig. 6). Further, our random forest models explain approximately 58 to 78% of the variation in the temporal trend of land cover change for croplands. In the case of other land cover types, the random forest models account for approximately 33-59% of the

variation in temporal trends of land cover change, with drought indices explaining less variation in land cover change for forests than other land cover types (Fig. 6).

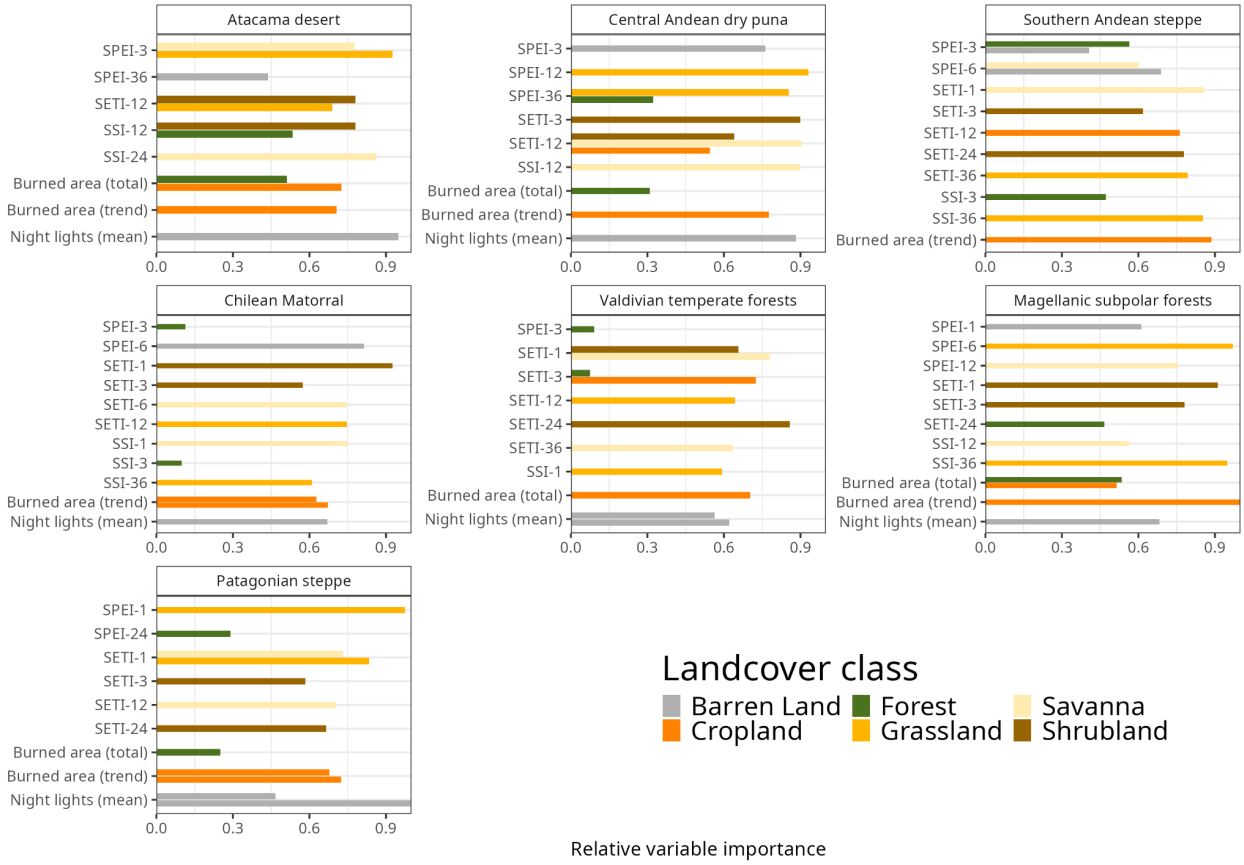

Figure 7. Drying trends are leading to changes in land cover. Variable importance of multi-scalar drought indices and human activity (i.e., night light emissions, road density, and fires) estimated by Random Forest models that explain variation in land cover change across ecoregions in continental Chile. Random Forest models were fitted for each combination of land cover type and time scale (1, 3, 6, 12, 24, and 36 months). SPEI is the Standardized Precipitation Evapotranspiration Index, SETI is the Standardized Evapotranspiration Index, SSI is the Standardized Soil Moisture Index, Night Lights(*) is the average nighttime light emissions for 2012-2023, Burned Area is the trend in surface burned for 2002-2023, and Burned Area(*) is the total surface affected by fires between 2002 and 2023. Note that we only show the two explanatory variables with the highest variable importance values for each land cover type and time scale.

We found the highest R^2 for the random forest model explaining variation in the temporal trend of land cover change for shrublands, followed by that for cropland and barren land (Fig. 6 & Figs. S12-S17). Our models most frequently identified SETI and SSI as the drought indices that explained the highest amount of variation in land cover change (Fig. 7).

Similarly, we found that nighttime light emissions, a proxy for human population and built structure density, explained relatively more variation in land cover change of barren land, followed by SPEI at time scales of 3 and 6 months (Fig. 7).

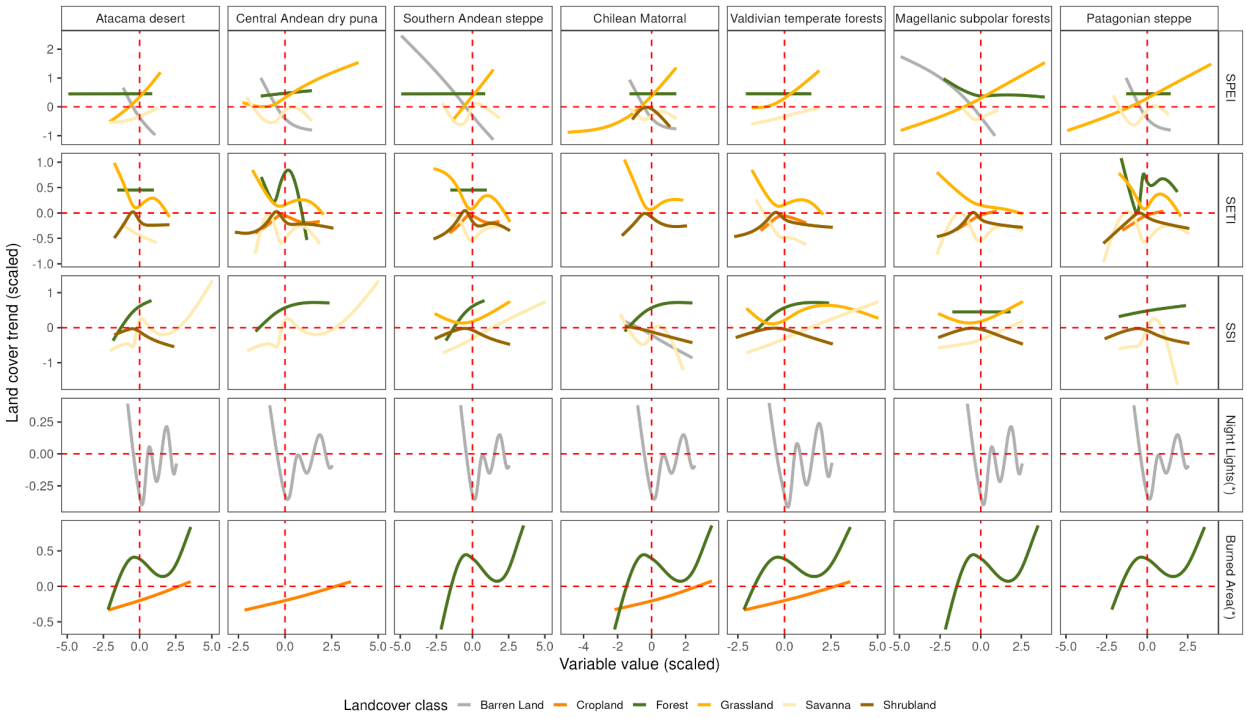

Figure 8. Drying trends drive land cover change, but not for all cover types. Response of land cover change in response to water demand and supply at multiple time scales and human activity (i.e., night light emissions, road density, and fires) across ecoregions in continental Chile. SPEI is the Standardized Precipitation Evapotranspiration Index, SETI is the Standardized Evapotranspiration Index, SSI is the Standardized Soil Moisture Index, Night Lights(*) is the average nighttime light emissions for 2012-2023, and Burned Area(*) is the total surface affected by fires between 2002 and 2023. For SPI, SPEI, SETI, and SSI, negative values are associated with more severe drought. Fitted lines are smoothed response curves in each ecoregion estimated with Random Forest models. Note that we only show the two explanatory variables with the highest variable importance values for each land cover type and time scale.

In general, our results indicate that increases in SPEI, SETI, and SSI were associated with non-linear increases in land cover change for most types of land cover (Fig. 8). We observed that shrublands are sensitive to both increases and decreases in SETI and SSI, reaching a point of equilibrium around normal levels of drought intensity, i.e., values close to zero. Surprisingly, we found that the temporal trend in the land cover change of forests

was stable for both SPEI and SETI for most ecoregions, only increasing non-linearly with increasing SSI. In the case of bare soil, we found a negative relationship between the temporal trend in land cover and nighttime light emissions, such that areas with an increase in barren land are associated with a low amount of nighttime light emissions (Fig. 8). We found that SETI and SPEI had contrasting impacts on land cover change of grasslands, which increased in response to increasing SPEI yet decreased in response to increasing SETI.

4. Discussion

4.1. Temporal trends in water supply and demand

We found that the Atacama desert, Central Andean dry puna, and the Magellanic subpolar forests experience an increase in water supply (SPI, SSI), as well as an increase in atmospheric and vegetation water demand (EDDI, SETI). However, in the Magellanic subpolar forests, we found no evidence of either a significant increase or decrease in SETI across time scales. Also, we found a significant decrease trend in water supply (SPI, SPEI, and SSI) across the Southern Andean steppe, Chilean Matorral (Boisier et al., 2018; Sarricolea et al., 2019), Valdivian temperate forests, and Patagonian steppe, accompanied by an increase in atmospheric water demand (EDDI). Our results indicate that water supply and atmospheric demand tend to decrease or increase more strongly over longer time scales, a trend that is consistent with the progressive intensification of aridification across much of Chile, and that has been observed in other regions facing long-term droughts (Miró et al., 2023; Overpeck & Udall, 2020; Rashid & Beecham, 2019). Simultaneously, we observed a divergent trend between EDDI and SETI. In the majority of ecoregions, a rise in atmospheric water demand (EDDI) typically leads to a rise in evapotranspiration (SETI). However, in the ecoregions most affected by drought (Figs. 3 & 5), i.e., the Chilean matorral and the Patagonian steppe, we found that an increase in atmospheric water demand is accompanied by a decrease in the water demand of vegetation. Together, our findings demonstrate a persistent drying trend in the Chilean Matorral, the Patagonian steppe, and the Southern Andean steppe. We attribute this trend to a simultaneous decrease in

precipitation and an increase in atmospheric evaporative demand, leading to a decrease in the water demand by vegetation in water-limited areas (Páscoa et al., 2021).

4.2. Temporal trends in vegetation productivity

The consequences of the persistent drying trend for ecosystems throughout continental Chile are manifold. First, the aridification, i.e., precipitation deficit and increase of AED, has leading to a steady decline in vegetation productivity (zcNDVI) since 2000 across the Patagonian steppe, the Southern Andean steppe, and the Chilean Matorral, which reached its lowest level between 2020 and 2022 and could be due to either a loss of biomass or browning in ecosystems (Miranda et al., 2020). Recent studies examining natural and productive ecosystems (Jiang et al., 2020; Nicolai-Shaw et al., 2017; Zhou et al., 2021) have attributed the decline in vegetation productivity with declines in soil moisture and increases in evapotranspiration. Second, the sharp decline in vegetation productivity in the Chilean Matorral and Valdivian temperate forest ecoregions showed that grasslands and shrublands respond to shifts in water supply over longer time scales (12 months) than savannas and croplands (6 months). Also, in the Valdivian temperate forest ecoregion, which has a large forested area, vegetation productivity responded to soil moisture (SSI) and evapotranspiration (SETI) most strongly at 12 and 36 months, respectively. This result is consistent with recent studies showing that progressive, long-term water deficits in central Chile have triggered forest browning and declines in native forest productivity (Miranda et al., 2020, 2023; Venegas-González et al., 2023). While our analysis does not distinguish between native and planted forests, the latter of which are considered to be more drought tolerant in central and southern Chile (Carrasco et al., 2022), we show that forest area declines more sharply in response to increasing water demand due to rising temperatures (EDDI) than decreasing water supply (e.g., SPI, SSI; (Fajardo et al., 2019; Holz et al., 2018). This could be explained by its deeper root system and the mixed types of forests; some trees may strictly close their stomata (which regulate water loss), while others might keep their stomata more open. This may also have cascading impacts on multiple facets of forest diversity (Sabatini et al., 2022; Segovia et al., 2020).

Moreover, the strengthening of the correlation between vegetation productivity and water supply (SPI, SPEI, SSI) or demand (EDDI, SETI) over multiple time scales (up to 36 months) and across land cover types (Fig. 5) demonstrates the impacts of climate change on the water balance across continental Chile. These impacts may extend beyond vegetation productivity, as reduced soil moisture in central Chile and the western United States has increased wildfire activity (González et al., 2018; Holden et al., 2018), which is a growing concern in Chile and may be further exacerbated by extensive plantations of highly flammable tree species, e.g., *Eucalyptus* spp. and *Pinus* spp. (Bowman et al., 2019). Lastly, we found that the decline in the vegetation productivity of croplands is largely associated with a decrease in the water supply and vegetation water demand with a greater extent than to an increase in atmospheric water demand (Quiring & Ganesh, 2010), causing a decline in water availability.

4.3. The impact of drying trends on land cover indicates aridification

We found evidence that temporal decreases in water supply (SPEI, SSI) and evapotranspiration (SETI) are strongly linked not only with vegetation productivity but also with temporal trends in land cover change across most of continental Chile. Despite differences in drought tolerance (e.g., shrublands, grasslands, and savannas), our results provide evidence that the area of most vegetation-dominated land cover types have been affected by water deficits, albeit to varying degrees (Fig. 8). Additionally, our results suggest that water deficits, to a greater extent than factors associated with human activity, have affected temporal trends in land cover change for most land cover types (e.g., croplands, forests, and infrastructure). Further, across all ecoregions, we found that the total surface of burned area or the temporal trend of burned area explained relatively more variation in the temporal trend of land cover change for cropland than drought indices, as well as other variables associated with human activity (Fig. 7). According to the definition that we used to recognize aridification, it is when the long-term drying leads to permanent changes, i.e., land cover change (Lisonbee et al., 2025). The long-term drying trends and their impact on the land cover change shown in this study indicate that Chile is facing an aridification process rather than a drought.

The observed land cover shifts carry urgent policy implications. Biodiversity loss from the replacement of forests and wetlands with shrublands undermines ecosystem resilience, while increased fire activity—exacerbated by flammable plantations—can entrench land degradation. These dynamics threaten ecosystem services and intensify socio-economic risks, from declining agricultural productivity to rising water conflicts, highlighting the need for integrated policies on conservation, fire management, and rural adaptation.

4.4. Study limitations

Our analysis of the impacts of water supply and demand on vegetation productivity and land cover change has several limitations. One of the principal limitations of this study is the use of secondary information. For instance, we used estimates of water supply and demand, such as ERA5L and MODIS, which, despite their improved precision, suffer from biases and uncertainties (Clelland et al., 2024; Gomis-Cebolla et al., 2023) in different areas or climatic conditions. In this study, we compared the ERA5L data with local climatic stations (see Table S2) to estimate bias and uncertainty, but future studies with a more local focus will need to improve the precision of these products by, for example, merging in situ with ERA5L (Kossieris et al., 2024). We used zcNDVI (Zambrano et al., 2018) (MODIS) as a proxy for vegetation productivity, which has proven to be a good estimate of NPP (see Fig. S1 and S2), but its quality varies between different types of vegetation (Turner et al., 2006).

A second limitation is that we used products that estimate land cover types using classification models, which are subject to quality errors (Stehman & Foody, 2019; Verburg et al., 2011). In addition, in our case we used macro-classes of land cover, where, for example, the different types of forests (e.g., monoculture, native forest) were pooled into the same land cover type. This approach may hinder our ability to understand the effects of aridification on the various subclasses within each land cover class. In terms of cropland, we could not distinguish between rainfed and irrigated areas using macro classes. However, in this study, we aimed to provide a broad overview at a large spatial scale, but acknowledge that using sub-classes of land cover types at finer spatial resolutions may help to better understand underlying mechanisms.

In our analysis of the impacts of drying trends on land cover change, we integrated proxies for human activity that also may affect land cover change. However, attributing land cover change to human activity and decisions is complex when using earth observation tools. While earth observation tools can analyze land cover change, whether a land cover type changes likely depends on a multitude of social and economic factors that are challenging to quantify (Jenner et al., 2024; Rindfuss et al., 2004) and necessitate the integration of social, natural, and geographic information sciences.

5. Conclusion

Our results indicate that long-term variations in water supply and demand are strongly associated with a permanent drying trend, which has consistently induced widespread, multi-dimensional impacts on vegetation productivity and temporal changes in land cover across a broad range of ecoregions in continental Chile. This evidence suggests that the "mega-drought" in Chile has turned into an aridification process. Nevertheless, in this study, we modeled trends in land cover using climate, human growth variables, and random forest models. We cannot yet attribute aridification causation to the drought indices (most important variables), even though they are strongly correlated with land cover changes. In future studies, we need to deepen our understanding of human influence on land cover and prove alternative modeling frameworks.

While drying may be a potential cause of shifts to more drought-tolerant vegetation types, such as shrublands, we also found that areas affected by fires were associated with increases in the area of croplands, highlighting the importance of socio-economic factors in shaping land use change dynamics. Our study enhances the current understanding about drought and aridification. This knowledge can aid in the development of context-specific adaptation strategies for agriculture, biodiversity conservation, and natural resource management.

Open Research

The codes generated during the current study are available in the GitHub repository, https://github.com/frzambra/article_aridification_Chile (Zambrano, 2025). The datasets

generated and/or analyzed during the current study are available in Zenodo (Zambrano, 2023a).

Conflict of interest declaration

The authors declare there are no conflicts of interest for this manuscript.

Acknowledgments

The National Research and Development Agency of Chile (ANID) funded this study through the drought emergency project FSEQ210022, Fondecyt Iniciación N°11190360, Fondecyt Postdoctorado N°3230678, and Fondecyt Regular N°1210526. We declare that the authors have no competing interests, or other interests that might be perceived to influence the results and/or discussion reported in this paper.

References

Abramowitz, M., & Stegun, I. A. (1968). *Handbook of mathematical functions with formulas, graphs, and mathematical tables* (Vol. 55). US Government printing office.

Aceituno, P., Boisier, J. P., Garreaud, R., Rondanelli, R., & Rutllant, J. A. (2021). Climate and Weather in Chile. In B. Fernández & J. Gironás (Eds.), *Water Resources of Chile* (Vol. 8, pp. 7–29). Springer International Publishing.

AghaKouchak, A. (2014). A baseline probabilistic drought forecasting framework using standardized soil moisture index: Application to the 2012 United States drought. *Hydrology and Earth System Sciences*, *18*(7), 2485–2492. https://doi.org/10.5194/hess-18-2485-2014

AghaKouchak, A., Farahmand, A., Melton, F. S., Teixeira, J., Anderson, M. C., Wardlow, B. D., & Hain, C. R. (2015). Remote sensing of drought: Progress, challenges and opportunities. *Reviews of Geophysics*, *53*(2), 452–480. https://doi.org/10.1002/2014RG000456

Beck, H. E., McVicar, T. R., Vergopolan, N., Berg, A., Lutsko, N. J., Dufour, A., Zeng, Z., Jiang, X., van Dijk, A. I. J. M., & Miralles, D. G. (2023). High-resolution (1 km) Köppen-Geiger maps for 1901–2099 based on constrained CMIP6 projections. *Scientific Data*, *10*(1). https://doi.org/10.1038/s41597-023-02549-6

Beguería, S., & Vicente-Serrano, S. M. (2023). *SPEI: Calculation of the Standardized Precipitation-Evapotranspiration Index*. https://CRAN.R-project.org/package=SPEI

Beguería, S., Vicente-Serrano, S. M., Reig, F., & Latorre, B. (2014). Standardized precipitation evapotranspiration index (SPEI) revisited: Parameter fitting, evapotranspiration models, tools, datasets and drought monitoring. *International Journal of Climatology*, *34*(10), 3001–3023. https://doi.org/10.1002/joc.3887

Berdugo, M., Delgado-Baquerizo, M., Soliveres, S., Hernández-Clemente, R., Zhao, Y., Gaitán, J. J., Gross, N., Saiz, H., Maire, V., Lehmann, A., Rillig, M. C., Solé, R. V., & Maestre, F. T. (2020). Global ecosystem thresholds driven by aridity. *Science*, *367*(6479), 787–790. https://doi.org/10.1126/science.aay5958

Boisier, J. P., Alvarez-Garreton, C., Cordero, R. R., Damiani, A., Gallardo, L., Garreaud, R. D., Lambert, F., Ramallo, C., Rojas, M., & Rondanelli, R. (2018). Anthropogenic drying in central-southern Chile evidenced by long-term observations and climate model simulations. *Elementa*, *6*(1), 74. https://doi.org/10.1525/elementa.328

Bowler, D. E., Bjorkman, A. D., Dornelas, M., Myers-Smith, I. H., Navarro, L. M., Niamir, A., Supp, S. R., Waldock, C., Winter, M., Vellend, M., Blowes, S. A., Böhning-Gaese, K., Bruelheide, H., Elahi, R., Antão, L. H., Hines, J., Isbell, F., Jones, H. P., Magurran, A. E., … Bates, A. E. (2020). Mapping human pressures on biodiversity across the planet uncovers anthropogenic threat complexes. *People and Nature*, *2*(2), 380–394.

https://doi.org/10.1002/pan3.10071

Bowman, D. M. J. S., Moreira-Muñoz, A., Kolden, C. A., Chávez, R. O., Muñoz, A. A., Salinas, F., González-Reyes, Á., Rocco, R., De La Barrera, F., Williamson, G. J., Borchers, N., Cifuentes, L. A., Abatzoglou, J. T., & Johnston, F. H. (2019). Human–environmental drivers and impacts of the globally extreme 2017 Chilean fires. *Ambio*, *48*(4), 350–362. https://doi.org/10.1007/s13280-018-1084-1

Calvin, K., Dasgupta, D., Krinner, G., Mukherji, A., Thorne, P. W., Trisos, C., Romero, J., Aldunce, P., Barrett, K., Blanco, G., Cheung, W. W. L., Connors, S., Denton, F., Diongue-Niang, A., Dodman, D., Garschagen, M., Geden, O., Hayward, B., Jones, C., … Péan, C. (2023). *IPCC, 2023: Climate Change 2023: Synthesis Report. Contribution of Working Groups I, II and III to the Sixth Assessment Report of the Intergovernmental Panel on Climate Change [Core Writing Team, H. Lee and J. Romero (eds.)]. IPCC, Geneva, Switzerland.* Intergovernmental Panel on Climate Change (IPCC). https://www.ipcc.ch/report/ar6/syr/

Camps-Valls, G., Campos-Taberner, M., Moreno-Martínez, Á., Walther, S., Duveiller, G., Cescatti, A., Mahecha, M. D., Muñoz-Marí, J., García-Haro, F. J., Guanter, L., Jung, M., Gamon, J. A., Reichstein, M., & Running, S. W. (2021). A unified vegetation index for quantifying the terrestrial biosphere. *Science Advances*, *7*(9), eabc7447. https://doi.org/10.1126/sciadv.abc7447

Carrasco, G., Almeida, A. C., Falvey, M., Olmedo, G. F., Taylor, P., Santibañez, F., & Coops, N. C. (2022). Effects of climate change on forest plantation productivity in Chile. *Global Change Biology*, *28*(24), 7391–7409. https://doi.org/10.1111/gcb.16418

Chen, Q., Timmermans, J., Wen, W., & Van Bodegom, P. M. (2023). Ecosystems threatened by

intensified drought with divergent vulnerability. *Remote Sensing of Environment*, *289*, 113512. https://doi.org/10.1016/j.rse.2023.113512

Cheng, Y., Oehmcke, S., Brandt, M., Rosenthal, L., Das, A., Vrieling, A., Saatchi, S., Wagner, F., Mugabowindekwe, M., Verbruggen, W., Beier, C., & Horion, S. (2024). Scattered tree death contributes to substantial forest loss in California. *Nature Communications*, *15*(1), 641. https://doi.org/10.1038/s41467-024-44991-z

Clelland, A. A., Marshall, G. J., & Baxter, R. (2024). Evaluating the performance of key ERA-Interim , ERA5 and ERA5-Land climate variables across Siberia. *International Journal of Climatology*, *44*(7), 2318–2342. https://doi.org/10.1002/joc.8456

Craine, J. M., Ocheltree, T. W., Nippert, J. B., Towne, E. G., Skibbe, A. M., Kembel, S. W., & Fargione, J. E. (2013). Global diversity of drought tolerance and grassland climate-change resilience. *Nature Climate Change*, *3*(1), 63–67. https://doi.org/10.1038/nclimate1634

Dakos, V., Matthews, B., Hendry, A. P., Levine, J., Loeuille, N., Norberg, J., Nosil, P., Scheffer, M., & De Meester, L. (2019). Ecosystem tipping points in an evolving world. *Nature Ecology & Evolution*, *3*(3), 355–362. https://doi.org/10.1038/s41559-019-0797-2

Didan, K. (2015). *MOD13A3 MODIS/Terra Vegetation Indices Monthly L3 Global 1km SIN Grid V006* [Dataset]. NASA EOSDIS Land Processes Distributed Active Archive Center. https://doi.org/10.5067/MODIS/MOD13A3.006

Didan, K. (2021). *MODIS/Terra Vegetation Indices Monthly L3 Global 1km SIN Grid V061* [Dataset]. NASA EOSDIS Land Processes Distributed Active Archive Center. https://doi.org/10.5067/MODIS/MOD13A3.061

Dinerstein, E., Olson, D., Joshi, A., Vynne, C., Burgess, N. D., Wikramanayake, E., Hahn, N.,

Palminteri, S., Hedao, P., Noss, R., Hansen, M., Locke, H., Ellis, E. C., Jones, B., Barber, C. V., Hayes, R., Kormos, C., Martin, V., Crist, E., … Saleem, M. (2017). An Ecoregion-Based Approach to Protecting Half the Terrestrial Realm. *BioScience*, *67*(6), 534–545. https://doi.org/10.1093/biosci/bix014

Dormann, C. F., Elith, J., Bacher, S., Buchmann, C., Carl, G., Carré, G., Marquéz, J. R. G., Gruber, B., Lafourcade, B., Leitão, P. J., Münkemüller, T., McClean, C., Osborne, P. E., Reineking, B., Schröder, B., Skidmore, A. K., Zurell, D., & Lautenbach, S. (2013). Collinearity: A review of methods to deal with it and a simulation study evaluating their performance. *Ecography*, *36*(1), 27–46. https://doi.org/10.1111/j.1600-0587.2012.07348.x

Fajardo, A., Gazol, A., Mayr, C., & Camarero, J. J. (2019). Recent decadal drought reverts warming-triggered growth enhancement in contrasting climates in the southern Andes tree line. *Journal of Biogeography*, *46*(7), 1367–1379. https://doi.org/10.1111/jbi.13580

FAO. (2022). *The State of the World's Forests 2022*. FAO. http://www.fao.org/documents/card/en/c/cb9360en

Farahmand, A., & AghaKouchak, A. (2015). A generalized framework for deriving nonparametric standardized drought indicators. *Advances in Water Resources*, *76*, 140–145. https://doi.org/10.1016/j.advwatres.2014.11.012

Francisco Zambrano Bigiarini. (2025). *frzambra/article_aridification_Chile: Scripts article aridification* (Version v1.0) [Computer software]. Zenodo. https://doi.org/10.5281/ZENODO.17200707

Friedl, M., & Sulla-Menashe, D. (2019). *MCD12Q1 MODIS/Terra+Aqua Land Cover Type Yearly*

L3 Global 500m SIN Grid V006 [Data set]. NASA EOSDIS Land Processes DAAC. https://doi.org/10.5067/MODIS/MCD12Q1.006

Garreaud, R., Alvarez-Garreton, C., Barichivich, J., Boisier, J. P., Christie, D., Galleguillos, M., LeQuesne, C., McPhee, J., & Zambrano-Bigiarini, M. (2017). The 2010-2015 mega drought in Central Chile: Impacts on regional hydroclimate and vegetation. *Hydrology and Earth System Sciences Discussions*, *2017*, 1–37. https://doi.org/10.5194/hess-2017-191

Garreaud, R. D. (2009). The Andes climate and weather. *Advances in Geosciences*, *22*, 3–11. https://doi.org/10.5194/adgeo-22-3-2009

Gebrechorkos, S. H., Peng, J., Dyer, E., Miralles, D. G., Vicente-Serrano, S. M., Funk, C., Beck, H. E., Asfaw, D. T., Singer, M. B., & Dadson, S. J. (2023). Global high-resolution drought indices for 1981–2022. *Earth System Science Data*, *15*(12), 5449–5466. https://doi.org/10.5194/essd-15-5449-2023

Gebrechorkos, S. H., Sheffield, J., Vicente-Serrano, S. M., Funk, C., Miralles, D. G., Peng, J., Dyer, E., Talib, J., Beck, H. E., Singer, M. B., & Dadson, S. J. (2025). Warming accelerates global drought severity. *Nature*. https://doi.org/10.1038/s41586-025-09047-2

Gomis-Cebolla, J., Rattayova, V., Salazar-Galán, S., & Francés, F. (2023). Evaluation of ERA5 and ERA5-Land reanalysis precipitation datasets over Spain (1951–2020). *Atmospheric Research*, *284*, 106606. https://doi.org/10.1016/j.atmosres.2023.106606

González, M. E., Gómez-González, S., Lara, A., Garreaud, R., & Díaz-Hormazábal, I. (2018). The 2010–2015 Megadrought and its influence on the fire regime in central and south-central Chile. *Ecosphere*, *9*(8), e02300. https://doi.org/10.1002/ecs2.2300

Halpern, B. S., Frazier, M., Potapenko, J., Casey, K. S., Koenig, K., Longo, C., Lowndes, J. S., Rockwood, R. C., Selig, E. R., Selkoe, K. A., & Walbridge, S. (2015). Spatial and temporal changes in cumulative human impacts on the world's ocean. *Nature Communications*, *6*(1), 7615. https://doi.org/10.1038/ncomms8615

Halpern, B. S., Walbridge, S., Selkoe, K. A., Kappel, C. V., Micheli, F., D'Agrosa, C., Bruno, J. F., Casey, K. S., Ebert, C., Fox, H. E., Fujita, R., Heinemann, D., Lenihan, H. S., Madin, E. M. P., Perry, M. T., Selig, E. R., Spalding, M., Steneck, R., & Watson, R. (2008). A Global Map of Human Impact on Marine Ecosystems. *Science*, *319*(5865), 948–952. https://doi.org/10.1126/science.1149345

Hao, Z., & AghaKouchak, A. (2013). Multivariate standardized drought index: {A} parametric multi-index model. *Advances in Water Resources*, *57*, 12–18.

Heim, R. R. (2002). A review of twentieth-century drought indices used in the united states. *American Meteorological Society*, *83*, 1149–1165.

Helman, D., Mussery, A., Lensky, I. M., & Leu, S. (2014). Detecting changes in biomass productivity in a different land management regimes in drylands using satellite-derived vegetation index. *Soil Use and Management*, *30*(1), 32–39. https://doi.org/10.1111/sum.12099

Hijmans, R. J. (2023). *terra: Spatial Data Analysis*. https://CRAN.R-project.org/package=terra

Ho, T. K. (1995). Random decision forests. *Proceedings of 3rd International Conference on Document Analysis and Recognition*, *1*, 278–282.

Hobbins, M. T., Wood, A., McEvoy, D. J., Huntington, J. L., Morton, C., Anderson, M., & Hain, C. (2016). The Evaporative Demand Drought Index. Part I: Linking Drought Evolution to

Variations in Evaporative Demand. *Journal of Hydrometeorology*, *17*(6), 1745–1761. https://doi.org/10.1175/JHM-D-15-0121.1

Holden, Z. A., Swanson, A., Luce, C. H., Jolly, W. M., Maneta, M., Oyler, J. W., Warren, D. A., Parsons, R., & Affleck, D. (2018). Decreasing fire season precipitation increased recent western US forest wildfire activity. *Proceedings of the National Academy of Sciences*, *115*(36). https://doi.org/10.1073/pnas.1802316115

Holz, A., Hart, S. J., Williamson, G. J., Veblen, T. T., & Aravena, J. C. (2018). Radial growth response to climate change along the latitudinal range of the world's southernmost conifer in southern South America. *Journal of Biogeography*, *45*(5), 1140–1152. https://doi.org/10.1111/jbi.13199

Hong, S., Deng, H., Zheng, Z., Deng, Y., Chen, X., Gao, L., Chen, Y., & Liu, M. (2023). The influence of variations in actual evapotranspiration on drought in China's Southeast River basin. *Scientific Reports*, *13*(1), 21336. https://doi.org/10.1038/s41598-023-48663-8

Hufkens, K., Stauffer, R., & Campitelli, E. (2019). *The ecwmfr package: An interface to ECMWF API endpoints*. https://bluegreen-labs.github.io/ecmwfr/

Jenner, L., Metzger, M., Moseley, D., Peskett, L., & Forrest, E. (2024). The limitations and risks of land use change tools in decision-making: Lessons from Galloway and Southern Ayrshire UNESCO Biosphere, Scotland. *Environmental Science & Policy*, *161*, 103889. https://doi.org/10.1016/j.envsci.2024.103889

Jiang, W., Wang, L., Feng, L., Zhang, M., & Yao, R. (2020). Drought characteristics and its impact on changes in surface vegetation from 1981 to 2015 in the Yangtze River Basin, China. *International Journal of Climatology*, *40*(7), 3380–3397.

https://doi.org/10.1002/joc.6403

Karabulut, A. İ., Yazıcı Karabulut, B., Demir Yetiş, A., Yeşilnacar, M. İ., & Derin, P. (2023). Socioeconomic driving forces of land use/cover changes in the semi-arid Harran plain and their probable implications on arising groundwater level, the GAP area of southeastern Türkiye. *Acta Geophysica*, *71*(6), 2795–2810. https://doi.org/10.1007/s11600-023-01162-w

Kennedy, C. M., Oakleaf, J. R., Theobald, D. M., Baruch-Mordo, S., & Kiesecker, J. (2019). Managing the middle: A shift in conservation priorities based on the global human modification gradient. *Global Change Biology*, *25*(3), 811–826. https://doi.org/10.1111/gcb.14549

Kossieris, P., Tsoukalas, I., Brocca, L., Mosaffa, H., Makropoulos, C., & Anghelea, A. (2024). Precipitation data merging via machine learning: Revisiting conceptual and technical aspects. *Journal of Hydrology*, *637*, 131424. https://doi.org/10.1016/j.jhydrol.2024.131424

Kuhn, M., & Wickham, H. (2020). *Tidymodels: A collection of packages for modeling and machine learning using tidyverse principles.* https://www.tidymodels.org

Laimighofer, J., & Laaha, G. (2022). How standard are standardized drought indices? Uncertainty components for the SPI & SPEI case. *Journal of Hydrology*, *613*, 128385. https://doi.org/10.1016/j.jhydrol.2022.128385

Li, W., Migliavacca, M., Forkel, M., Denissen, J. M. C., Reichstein, M., Yang, H., Duveiller, G., Weber, U., & Orth, R. (2022). Widespread increasing vegetation sensitivity to soil moisture. *Nature Communications*, *13*(1), 3959. https://doi.org/10.1038/s41467-022-31667-9

Lisonbee, J., Parker, B., Fleishman, E., Ford, T. W., Bocinsky, R. K., Follingstad, G., Frazier, A. G., Hoylman, Z. H., Hudson, A. R., Nielsen-Gammon, J. W., Umphlett, N. A., Wickham, E., Bamzai-Dodson, A., Fontenot, R., Fuchs, B., Hammond, J., Herrick, J. E., Hobbins, M., Hoell, A., … Pulwarty, R. (2025). Prioritization of Research on Drought Assessment in a Changing Climate. *Earth's Future*, *13*(3), e2024EF005276. https://doi.org/10.1029/2024EF005276

Liu, L., Gudmundsson, L., Hauser, M., Qin, D., Li, S., & Seneviratne, S. I. (2020). Soil moisture dominates dryness stress on ecosystem production globally. *Nature Communications 2020 11:1*, *11*(1), 1–9. https://doi.org/10.1038/s41467-020-18631-1

Liu, X., Yu, S., Yang, Z., Dong, J., & Peng, J. (2024). The first global multi-timescale daily SPEI dataset from 1982 to 2021. *Scientific Data*, *11*(1), 223. https://doi.org/10.1038/s41597-024-03047-z

Luebert, F., & Pliscoff, P. (2022). The vegetation of Chile and the EcoVeg approach in the context of the International Vegetation Classification project. *Vegetation Classification and Survey*, *3*, 15–28. https://doi.org/10.3897/VCS.67893

Marumbwa, F. M., Cho, M. A., & Chirwa, P. W. (2020). An assessment of remote sensing-based drought index over different land cover types in southern Africa. *International Journal of Remote Sensing*, *41*(19), 7368–7382. https://doi.org/10.1080/01431161.2020.1757783

McDowell, N. G., Sapes, G., Pivovaroff, A., Adams, H. D., Allen, C. D., Anderegg, W. R. L., Arend, M., Breshears, D. D., Brodribb, T., Choat, B., Cochard, H., De Cáceres, M., De Kauwe, M. G., Grossiord, C., Hammond, W. M., Hartmann, H., Hoch, G., Kahmen, A., Klein, T., … Xu, C. (2022). Mechanisms of woody-plant mortality under rising drought, CO2 and

vapour pressure deficit. *Nature Reviews Earth & Environment*, *3*(5), 294–308. https://doi.org/10.1038/s43017-022-00272-1

McEvoy, D. J., Huntington, J. L., Hobbins, M. T., Wood, A., Morton, C., Anderson, M., & Hain, C. (2016). The Evaporative Demand Drought Index. Part II: CONUS-Wide Assessment against Common Drought Indicators. *Journal of Hydrometeorology*, *17*(6), 1763–1779. https://doi.org/10.1175/JHM-D-15-0122.1

Mckee, T. B., Doesken, N. J., & Kleist, J. (1993). The relationship of drought frequency and duration to time scales. In: Proceedings of the Ninth Conference on Applied Climatology. *American Metereological Society*, *Boston*, 179–184.

McKee, T. B., Doesken, N. J., Kleist, J., & Society, A. M. (1995). *Drought Monitoring with Multiple Time Scales*. The Society.

Meijer, J. R., Huijbregts, M. A. J., Schotten, K. C. G. J., & Schipper, A. M. (2018). Global patterns of current and future road infrastructure. *Environmental Research Letters*, *13*(6), 064006. https://doi.org/10.1088/1748-9326/aabd42

Miranda, A., Lara, A., Altamirano, A., Di Bella, C., González, M. E., & Julio Camarero, J. (2020). Forest browning trends in response to drought in a highly threatened mediterranean landscape of South America. *Ecological Indicators*, *115*, 106401. https://doi.org/10.1016/j.ecolind.2020.106401

Miranda, A., Syphard, A. D., Berdugo, M., Carrasco, J., Gómez-González, S., Ovalle, J. F., Delpiano, C. A., Vargas, S., Squeo, F. A., Miranda, M. D., Dobbs, C., Mentler, R., Lara, A., & Garreaud, R. (2023). Widespread synchronous decline of Mediterranean-type forest driven by accelerated aridity. *Nature Plants*, *9*(11), 1810–1817. https://doi.org/10.1038/s41477-023-01541-7

Miró, J. J., Estrela, M. J., Corell, D., Gómez, I., & Luna, M. Y. (2023). Precipitation and drought trends (1952–2021) in a key hydrological recharge area of the eastern Iberian Peninsula. *Atmospheric Research*, *286*, 106695. https://doi.org/10.1016/j.atmosres.2023.106695

Mirzabaev, A., Stringer, L. C., Benjaminsen, T. A., Gonzalez, P., Harris, R., Jafari, M., Stevens, N., Tirado, C. M., & Zakieldeen, S. (2022). Cross-Chapter Paper 3: Deserts, Semiarid Areas and Desertification. In H.-O. Pörtner, D. C. Roberts, M. Tignor, E. S. Poloczanska, K. Mintenbeck, A. Alegría, M. Craig, S. Langsdorf, S. Löschke, V. Möller, A. Okem, & B. Rama (Eds.), *Climate Change 2022: Impacts, Adaptation and Vulnerability. Contribution of Working Group II to the Sixth Assessment Report of the Intergovernmental Panel on Climate Change* (pp. 2195–2231). Cambridge University Press. https://doi.org/10.1017/9781009325844.020

Moss, W. E., Crausbay, S. D., Rangwala, I., Wason, J. W., Trauernicht, C., Stevens-Rumann, C. S., Sala, A., Rottler, C. M., Pederson, G. T., Miller, B. W., Magness, D. R., Littell, J. S., Frelich, L. E., Frazier, A. G., Davis, K. T., Coop, J. D., Cartwright, J. M., & Booth, R. K. (2024). Drought as an emergent driver of ecological transformation in the twenty-first century. *BioScience*, *74*(8), 524–538. https://doi.org/10.1093/biosci/biae050

Muñoz-Sabater, J., Dutra, E., Agustí-Panareda, A., Albergel, C., Arduini, G., Balsamo, G., Boussetta, S., Choulga, M., Harrigan, S., Hersbach, H., Martens, B., Miralles, D. G., Piles, M., Rodríguez-Fernández, N. J., Zsoter, E., Buontempo, C., & Thépaut, J.-N. (2021). ERA5-Land: A state-of-the-art global reanalysis dataset for land applications. *Earth System Science Data*, *13*(9), 4349–4383. https://doi.org/10.5194/essd-13-4349-2021

Narasimhan, B., & Srinivasan, R. (2005). Development and evaluation of Soil Moisture Deficit Index (SMDI) and Evapotranspiration Deficit Index (ETDI) for agricultural drought monitoring. *Agricultural and Forest Meteorology*, *133*(1–4), 69–88. https://doi.org/10.1016/j.agrformet.2005.07.012

Nicolai-Shaw, N., Zscheischler, J., Hirschi, M., Gudmundsson, L., & Seneviratne, S. I. (2017). A drought event composite analysis using satellite remote-sensing based soil moisture. *Remote Sensing of Environment*, *203*, 216–225. https://doi.org/10.1016/j.rse.2017.06.014

Overpeck, J. T., & Udall, B. (2020). Climate change and the aridification of North America. *Proceedings of the National Academy of Sciences*, *117*(22), 11856–11858. https://doi.org/10.1073/pnas.2006323117

Paruelo, J. M., Texeira, M., Staiano, L., Mastrángelo, M., Amdan, L., & Gallego, F. (2016). An integrative index of Ecosystem Services provision based on remotely sensed data. *Ecological Indicators*, *71*, 145–154. https://doi.org/10.1016/j.ecolind.2016.06.054

Páscoa, P., Russo, A., Gouveia, C. M., Soares, P. M. M., Cardoso, R. M., Careto, J. A. M., & Ribeiro, A. F. S. (2021). A high-resolution view of the recent drought trends over the Iberian Peninsula. *Weather and Climate Extremes*, *32*, 100320. https://doi.org/10.1016/j.wace.2021.100320

Pebesma, E. (2018). Simple Features for R: Standardized Support for Spatial Vector Data. *The R Journal*, *10*(1), 439–446. https://doi.org/10.32614/RJ-2018-009

Pebesma, E., & Bivand, R. (2023). *Spatial Data Science: With applications in R*. Chapman and Hall/CRC. https://r-spatial.org/book/

Peng, D., Zhang, B., Wu, C., Huete, A. R., Gonsamo, A., Lei, L., Ponce-Campos, G. E., Liu, X., &

Wu, Y. (2017). Country-level net primary production distribution and response to drought and land cover change. *Science of The Total Environment*, *574*, 65–77. https://doi.org/10.1016/j.scitotenv.2016.09.033

Pricope, N. G., Vicente-Serrano, S. M., Toreti, A., Ocampo-Melgar, A., Spinoni, J., Morán-Tejeda, E., Archer, E., Diedhiou, A., Ravindranath, N., Mesbahzadeh, T., Pulwarty, R. S., & Alibakhshi, S. (2025). Increasing aridification calls for urgent global adaptive solutions and policy action. *Nature Water*, *3*(5), 512–515. https://doi.org/10.1038/s44221-025-00432-9

Quiring, S. M., & Ganesh, S. (2010). Evaluating the utility of the Vegetation Condition Index (VCI) for monitoring meteorological drought in Texas. *Agricultural and Forest Meteorology*, *150*(3), 330–339. https://doi.org/10.1016/j.agrformet.2009.11.015

R Core Team. (2025). *R: A Language and Environment for Statistical Computing*. R Foundation for Statistical Computing. https://www.R-project.org/

Rashid, M. M., & Beecham, S. (2019). Characterization of meteorological droughts across South Australia. *Meteorological Applications*, *26*(4), 556–568. https://doi.org/10.1002/met.1783

Rindfuss, R. R., Walsh, S. J., Turner, B. L., Fox, J., & Mishra, V. (2004). Developing a science of land change: Challenges and methodological issues. *Proceedings of the National Academy of Sciences*, *101*(39), 13976–13981. https://doi.org/10.1073/pnas.0401545101

Román, M. O., Wang, Z., Sun, Q., Kalb, V., Miller, S. D., Molthan, A., Schultz, L., Bell, J., Stokes, E. C., Pandey, B., Seto, K. C., Hall, D., Oda, T., Wolfe, R. E., Lin, G., Golpayegani, N., Devadiga, S., Davidson, C., Sarkar, S., … Masuoka, E. J. (2018). NASA's Black Marble

nighttime lights product suite. *Remote Sensing of Environment*, *210*, 113–143. https://doi.org/10.1016/j.rse.2018.03.017

Running, S., Mu, Q., & Zhao, M. (2017). *MOD16A2 MODIS/Terra Net Evapotranspiration 8-Day L4 Global 500m SIN Grid V006* [Dataset]. NASA EOSDIS Land Processes Distributed Active Archive Center. https://doi.org/10.5067/MODIS/MOD16A2.006

Running, S., & Zhao, M. (2019). *MOD17A3HGF MODIS/Terra Net Primary Production Gap-Filled Yearly L4 Global 500 m SIN Grid V006* [Dataset]. [object Object]. https://doi.org/10.5067/MODIS/MOD17A3HGF.006

Sabatini, F. M., Jiménez-Alfaro, B., Jandt, U., Chytrý, M., Field, R., Kessler, M., Lenoir, J., Schrodt, F., Wiser, S. K., Arfin Khan, M. A. S., Attorre, F., Cayuela, L., De Sanctis, M., Dengler, J., Haider, S., Hatim, M. Z., Indreica, A., Jansen, F., Pauchard, A., … Bruelheide, H. (2022). Global patterns of vascular plant alpha diversity. *Nature Communications*, *13*(1), 4683. https://doi.org/10.1038/s41467-022-32063-z

Sarricolea, P., Meseguer-Ruiz, Ó., Serrano-Notivoli, R., Soto, M. V., & Martin-Vide, J. (2019). Trends of daily precipitation concentration in Central-Southern Chile. *Atmospheric Research*, *215*, 85–98. https://doi.org/10.1016/j.atmosres.2018.09.005

Scholes, R., Montanarella, L., Brainich, A., Barger, N., ten Brink, B., Cantele, M., Erasmus, B., Fisher, J., Gardner, T., Holland, T. G., Kohler, F., Kotiaho, J. S., Von Maltitz, G., Nangendo, G., Pandit, R., Parrotta, J., Potts, M. D., Prince, S., Sankaran, M., & Willemen, L. (Eds.). (2018). *Summary for policymakers of the assessment report on land degradation and restoration of the Intergovernmental Science-Policy Platform on Biodiversity and Ecosystem Services*. IPBES Secretariat.

Segovia, R. A., Pennington, R. T., Baker, T. R., Coelho De Souza, F., Neves, D. M., Davis, C. C.,

Armesto, J. J., Olivera-Filho, A. T., & Dexter, K. G. (2020). Freezing and water availability structure the evolutionary diversity of trees across the Americas. *Science Advances*, *6*(19), eaaz5373. https://doi.org/10.1126/sciadv.aaz5373

Sen, P. K. (1968). Estimates of the Regression Coefficient Based on Kendall's Tau. *Journal of the American Statistical Association*, *63*(324), 1379–1389. https://doi.org/10.1080/01621459.1968.10480934

Shukla, P. R., Skea, J., Calvo Buendia, E., Masson-Delmotte, V., Pörtner, H.-O., Roberts, D. C., Zhai, P., Slade, R., Connors, S., van Diemen, R., Ferrat, M., Haughey, E., Luz, S., Neogi, S., Pathak, M., Petzold, J., Portugal Pereira, J., Vyas, P., Huntley, E., … Malley, J. (Eds.). (2019). *Climate Change and Land: An IPCC Special Report on Climate Change, Desertification, Land Degradation, Sustainable Land Management, Food Security, and Greenhouse Gas Fluxes in Terrestrial Ecosystems*. Intergovernmental Panel on Climate Change. https://www.ipcc.ch/srccl/

Souza, A. G. S. S., Ribeiro Neto, A., & Souza, L. L. D. (2021). Soil moisture-based index for agricultural drought assessment: SMADI application in Pernambuco State-Brazil. *Remote Sensing of Environment*, *252*, 112124. https://doi.org/10.1016/j.rse.2020.112124

Stehman, S. V., & Foody, G. M. (2019). Key issues in rigorous accuracy assessment of land cover products. *Remote Sensing of Environment*, *231*, 111199. https://doi.org/10.1016/j.rse.2019.05.018

Tennekes, M. (2018). tmap: Thematic Maps in R. *Journal of Statistical Software*, *84*(6), 1–39. https://doi.org/10.18637/jss.v084.i06

Tollerud, H., Brown, J., Loveland, T., Mahmood, R., & Bliss, N. (2018). Drought and

Land-Cover Conditions in the Great Plains. *Earth Interactions*, *22*(17), 1–25. https://doi.org/10.1175/EI-D-17-0025.1

Turner, D. P., Ritts, W. D., Cohen, W. B., Gower, S. T., Running, S. W., Zhao, M., Costa, M. H., Kirschbaum, A. A., Ham, J. M., Saleska, S. R., & Ahl, D. E. (2006). Evaluation of MODIS NPP and GPP products across multiple biomes. *Remote Sensing of Environment*, *102*(3–4), 282–292. https://doi.org/10.1016/j.rse.2006.02.017

Urrutia-Jalabert, R., González, M. E., González-Reyes, Á., Lara, A., & Garreaud, R. (2018). Climate variability and forest fires in central and south-central Chile. *Ecosphere*, *9*(4), e02171. https://doi.org/10.1002/ecs2.2171

Venegas-González, A., Juñent, F. R., Gutiérrez, A. G., & Filho, M. T. (2018). Recent radial growth decline in response to increased drought conditions in the northernmost Nothofagus populations from South America. *Forest Ecology and Management*, *409*, 94–104. https://doi.org/10.1016/j.foreco.2017.11.006

Venegas-González, A., Muñoz, A. A., Carpintero-Gibson, S., González-Reyes, A., Schneider, I., Gipolou-Zuñiga, T., Aguilera-Betti, I., & Roig, F. A. (2023). Sclerophyllous Forest Tree Growth Under the Influence of a Historic Megadrought in the Mediterranean Ecoregion of Chile. *Ecosystems*, *26*(2), 344–361. https://doi.org/10.1007/s10021-022-00760-x

Verburg, P. H., Neumann, K., & Nol, L. (2011). Challenges in using land use and land cover data for global change studies. *Global Change Biology*, *17*(2), 974–989. https://doi.org/10.1111/j.1365-2486.2010.02307.x

Vicente-Serrano, S. M., Azorin-Molina, C., Sanchez-Lorenzo, A., Revuelto, J., López-Moreno, J. I., González-Hidalgo, J. C., Moran-Tejeda, E., & Espejo, F. (2014). Reference

evapotranspiration variability and trends in Spain, 1961–2011. *Global and Planetary Change*, *121*, 26–40. https://doi.org/10.1016/j.gloplacha.2014.06.005

Vicente-Serrano, S. M., Beguería, S., & López-Moreno, J. I. (2010). A multiscalar drought index sensitive to global warming: The standardized precipitation evapotranspiration index. *Journal of Climate*, *23*(7), 1696–1718. https://doi.org/10.1175/2009JCLI2909.1

Vicente-Serrano, S. M., Domínguez-Castro, F., Beguería, S., El Kenawy, A., Gimeno-Sotelo, L., Franquesa, M., Azorin-Molina, C., Andres-Martin, M., & Halifa-Marín, A. (2025). Atmospheric drought indices in future projections. *Nature Water*, *3*(4), 374–387. https://doi.org/10.1038/s44221-025-00416-9

Vicente-Serrano, S. M., McVicar, T. R., Miralles, D. G., Yang, Y., & Tomas-Burguera, M. (2019). Unraveling the influence of atmospheric evaporative demand on drought and its response to climate change. *WIREs Climate Change*. https://doi.org/10.1002/wcc.632

Vicente-Serrano, S. M., Pricope, N. G., Toreti, A., Morán-Tejeda, E., Spinoni, J., Ocampo-Melgar, A., Archer, E., Diedhiou, A., Mesbahzadeh, T., Ravindranath, N. H., Pulwarty, R. S., & Alibakhshi, S. (2024). The United Nations Convention to Combat Desertification Report on Rising Aridity Trends Globally and Associated Biological and Agricultural Implications. *Global Change Biology*, *30*(12), e70009. https://doi.org/10.1111/gcb.70009

Wickham, H., Averick, M., Bryan, J., Chang, W., McGowan, L. D., François, R., Grolemund, G., Hayes, A., Henry, L., Hester, J., Kuhn, M., Pedersen, T. L., Miller, E., Bache, S. M., Müller, K., Ooms, J., Robinson, D., Seidel, D. P., Spinu, V., … Yutani, H. (2019). Welcome to the

tidyverse. *Journal of Open Source Software*, *4*(43), 1686. https://doi.org/10.21105/joss.01686

Wilks, D. S. (2011). Empirical distributions and exploratory data analysis. *Statistical Methods in the Atmospheric Sciences*, *100*.

Winkler, K., Fuchs, R., Rounsevell, M., & Herold, M. (2021). Global land use changes are four times greater than previously estimated. *Nature Communications*, *12*(1), 2501. https://doi.org/10.1038/s41467-021-22702-2

WMO, Svoboda, M., Hayes, M., & Wood, D. A. (2012). *Standardized Precipitation Index User Guide*. WMO.

Wright, M. N., & Ziegler, A. (2017). ranger: A Fast Implementation of Random Forests for High Dimensional Data in C++ and R. *Journal of Statistical Software*, *77*(1), 1–17. https://doi.org/10.18637/jss.v077.i01

Yue, S., & Wang, C. (2004). The Mann-Kendall Test Modified by Effective Sample Size to Detect Trend in Serially Correlated Hydrological Series. *Water Resources Management*, *18*(3), 201–218. https://doi.org/10.1023/B:WARM.0000043140.61082.60

Zambrano, F. (2023a). *Data of monthly climate variables and drought indices within continental Chile for 1981-2023* (Version 1.0) [Dataset]. Zenodo. https://doi.org/10.5281/ZENODO.10359547

Zambrano, F. (2023b). Four decades of satellite data for agricultural drought monitoring throughout the growing season in Central Chile. In R. M. Vijay P. Singh Deepak Jhajharia & R. Kumar (Eds.), *Integrated Drought Management, Two Volume Set* (p. 28). CRC Press.

Zambrano, F. (2025). *frzambra/article_aridification_Chile: Scripts article aridification* (Version v1.0) [Computer software]. Zenodo. https://doi.org/10.5281/ZENODO.17200707

Zambrano, F., Lillo-Saavedra, M., Verbist, K., & Lagos, O. (2016). Sixteen years of agricultural drought assessment of the biobío region in chile using a 250 m resolution vegetation condition index (VCI). *Remote Sensing*, *8*(6), 1–20. https://doi.org/10.3390/rs8060530

Zambrano, F., Vrieling, A., Nelson, A., Meroni, M., & Tadesse, T. (2018). Prediction of drought-induced reduction of agricultural productivity in Chile from MODIS, rainfall estimates, and climate oscillation indices. *Remote Sensing of Environment*, *219*, 15–30. https://doi.org/10.1016/j.rse.2018.10.006

Zhao, Y., Feng, D., Yu, L., Wang, X., Chen, Y., Bai, Y., Hernández, H. J., Galleguillos, M., Estades, C., Biging, G. S., Radke, J. D., & Gong, P. (2016). Detailed dynamic land cover mapping of Chile: Accuracy improvement by integrating multi-temporal data. *Remote Sensing of Environment*, *183*, 170–185. https://doi.org/10.1016/j.rse.2016.05.016

Zhou, K., Li, J., Zhang, T., & Kang, A. (2021). The use of combined soil moisture data to characterize agricultural drought conditions and the relationship among different drought types in China. *Agricultural Water Management*, *243*, 106479. https://doi.org/10.1016/j.agwat.2020.106479